Cancer Letters 625 (2025) 217736

Contents lists available at ScienceDirect

Cancer Letters

journal homepage: www.elsevier.com/locate/canlet

Original Articles

Mutant p53 confers chemoresistance by activating KMT5B-mediated DNA repair pathway in nasopharyngeal carcinoma

Haidan Luo [a,b], Mo-Fan Huang [a,c,1], An Xu [a,1], Donghui Wang [a,b,1], Julian A. Gingold [d], Jian Tu [a], Ruoyu Wang [c,e], Zijun Huo [a], Yen-Ting Chiang [a,h], Kuang-Lei Tsai [c,e], Jie Su [f], Danielle A. Bazer [g], Mien-Chie Hung [h,i], Canmao Xie [j], Yubiao Guo [j], Dung-Fang Lee [a,c,k,***], Huiling Yang [b,**], Ruiying Zhao [a,*]

[a] Department of Integrative Biology & Pharmacology, McGovern Medical School, The University of Texas Health Science Center at Houston, Houston, TX, 77030, USA
[b] Department of Pathophysiology, Zhongshan School of Medicine, Sun Yat-Sen University, Guangzhou, 510080, PR China
[c] The University of Texas MD Anderson Cancer Center UTHealth Houston Graduate School of Biomedical Sciences, Houston, TX, 77030, USA
[d] Department of Obstetrics & Gynecology and Women's Health. Einstein/Montefiore Medical Center, Bronx, NY, 10461, USA
[e] Department of Biochemistry and Molecular Biology, McGovern Medical School, The University of Texas Health Science Center at Houston, Houston, TX, 77030, USA
[f] Accutar Biotech, Brooklyn, NY, 11226, USA
[g] Department of Neurology, Renaissance School of Medicine at Stony Brook University. Stony Brook, NY, 11794, USA
[h] Graduate Institute of Biomedical Sciences and Center for Molecular Medicine, and Office of the President, China Medical University, Taichung, 404, Taiwan
[i] Department of Biotechnology, Asia University, Taichung, 413, Taiwan
[j] Division of Pulmonary and Critical Care Medicine, The First Affiliated Hospital of Sun Yat-sen University, Guangzhou, 510080, PR China
[k] Center for Precision Health, School of Biomedical Informatics, The University of Texas Health Science Center at Houston, Houston, TX, 77030, USA

ARTICLE INFO

Keywords:
Nasopharyngeal carcinoma
Mutant p53
KMT5B
5-FU
Chemoresistance
DNA repair
Curcumin

ABSTRACT

Nasopharyngeal carcinoma (NPC), a malignancy arising from the nasopharyngeal epithelium, is common in the east and southeast area of Asia. Treatments for locally advanced and recurrent NPC include chemotherapy (usually combined with 5-Fluorouracil, 5-FU) and radiotherapy, but response is limited due to chemo-resistance. p53 mutation is a critical factor for 5-FU resistance in some cancers, but its role in NPC chemo-resistance remains unclear. Here, we demonstrate that p53(R280T), a common p53 somatic mutation found in multiple NPC tumor samples, induces gain-of-function upregulation of DNA repair genes which leads to 5-FU resistance in NPC. p53 (R280T) specifically upregulates the expression of DNA repair-associated gene KMT5B by binding to its promoter, which leads to 5-FU resistance. Depletion of KMT5B in NPCs restores 5-FU induced DNA damages and improve the efficacy of 5-FU. By screening compounds affecting KMT5B expression, we identify curcumin as an effective down-regulator of KMT5B in NPC cells. We therefore evaluate the therapeutic potential of a 5-FU/curcumin combination to treat NPC and discover that curcumin enhances the efficacy of 5-FU to suppress NPC tumor growth. In summary, our findings indicate that mutant p53 and its regulated DNA repair genes serve as potential therapeutic targets to reverse 5-FU resistance for NPC patients.

1. Introduction

Nasopharyngeal carcinoma (NPC) is an epithelial carcinoma arising from the nasopharynx. In contrast to other epithelial head and neck tumors, the distribution of NPC cases is highly geographically dependent. According to the International Agency for Research on Cancer, although NPC accounted for 0.6 % (120,416 new cases) of all cancers diagnosed in 2022, NPCs are particularly prevalent in Hong-Kong and southern China [1]. Moreover, first-generation southern Chinese immigrants living in non-endemic regions such as the United States

* Corresponding author.
** Corresponding author.
*** Corresponding author. Department of Integrative Biology & Pharmacology, McGovern Medical School, The University of Texas Health Science Center at Houston, Houston, TX, 77030, USA.
E-mail addresses: dung-fang.lee@uth.tmc.edu (D.-F. Lee), yanghl@mail.sysu.edu.cn (H. Yang), ruiying.Zhao@uth.tmc.edu (R. Zhao).
[1] These authors contributed equally to this work.

https://doi.org/10.1016/j.canlet.2025.217736
Received 30 January 2025; Received in revised form 11 April 2025; Accepted 19 April 2025
Available online 30 April 2025

are at increased risk of NPC compared with the local population [2,3]. The World Health Organization classifies NPC into three pathological subtypes: keratinizing squamous, non-keratinizing, and basaloid squamous [4]. Of these, non-keratinizing NPC represents the largest share of cases in endemic areas and is strongly associated with Epstein-Barr virus (EBV) infection [5–7]. Recent studies exploring the molecular landscape of NPC revealed the crucial role of genomic alterations, including *TP53* mutations, in disease progression [8–10].

The p53 tumor suppressor is a DNA sequence-specific transcription factor that controls cell cycle arrest, cell death, and senescence through the transcriptional transactivation of its downstream target genes following cellular stress, such as DNA damage or oncogene-induced replication stress [11–13]. Under physiological conditions, p53 plays a vital role in facilitating DNA repair by inducing the expression of DNA repair genes and halting the cell cycle to allow time for the repair process [14]. In light of its crucial role in guarding genome integrity, p53 mutations have been strongly associated with the initiation and progression of a host of cancers [15–19]. Furthermore, p53 mutations are implicated in supporting chemoresistance in several cancers, such as colorectal cancer, lung cancer, and breast cancer [20–22]. The majority of p53 mutations are missense mutations in the DNA-binding domain (DBD), resulting in structural changes that impair p53's DNA-binding ability, which is required for transcriptional activation [13]. In addition to the abrogation of tumor suppressor functions, several p53 gain-of-function mutants have been shown to transcriptionally upregulate the chromatin regulators MLL1, MLL2, and MOZ [23], as well as directly interact with MLL1 to hijack H3K4me3 modifications [24,25], culminating in an oncogenic phenotype. p53 mutants have also been shown to induce gain-of-function activities, which compromise the efficacy of chemotherapy [22,26,27]. Whole-exome sequencing has identified recurrent p53 mutations, such as p53(R280T), in NPC [8,9]. Compromised p53 function increases dependence on glycolysis in p53-mutant cells, which further leads to increased sensitivity to ionizing radiation when combined with inhibition of glycolysis [28]. While some gain-of-function p53 mutant variants, such as p53(R248L), and the activated PI3K/mTOR pathway are important mediators of cisplatin resistance in squamous cell carcinomas of the head and neck [29], the authentic role of these p53 mutations in facilitating chemoresistance remains unclear.

KMT5B (lysine methyltransferase 5B, also known as SUV4-20H1) encodes a protein with a SET domain that functions as a histone methyltransferase [30]. KMT5B plays a crucial role in early mammalian development. Several studies have identified KMT5B as an important causative gene for autism spectrum disorder and other neurodevelopmental conditions [31]. Furthermore, KMT5B mediates H4K20 dimethylation (H4K20me2) and trimethylation (H4K20me3), which leads to transcriptional inhibition. These histone modifications are implicated in the repair of DNA damage, such as double-strand breaks (DSBs), caused by both endogenous (e.g., gene transcription) and exogenous stimuli (e.g., chemotherapy and radiation) [32]. A reduction in H4K20me2 caused by KMT5B deficiency impairs 53BP1-mediated DNA repair, resulting in elevated p53 expression and activation of its target gene Ddit4 (also known as Redd1), which has been linked to synaptic impairment [33]. Although accumulating evidence suggests a link between KMT5B and cancer progression [34], it remains unclear whether KMT5B is involved in mutant p53-driven tumor growth and chemoresistance.

According to the National Comprehensive Cancer Network (NCCN) Guidelines, while radiotherapy is the main therapeutic strategy for early-stage NPC, concurrent chemoradiotherapy, combining radiotherapy with systemic chemotherapy, is recommended as the mainstay treatment for locoregionally advanced, recurring, and distantly metastatic NPC due to its significant improvement in overall survival compared with radiotherapy [35–37]. 5-Fluorouracil (5-FU) in combination with docetaxel and cisplatin-based induction chemotherapy have been considered the first-line treatments for patients with advanced NPC [35,37,38]. Prior work has indicated that the primary anti-cancer activity of 5-FU arises through the upregulation of p53-activated DNA damage response and apoptosis-regulatory pathways [39]. However, a substantial proportion of NPC patients experience treatment failure and show tumor recurrence or distant metastasis due to chemoresistance [40,41]. Although several molecular events have been found to support the chemoresistance of NPC [42–44], an understanding of the detailed mechanisms in the development of 5-FU-associated chemoresistance in NPC remains unclear.

Curcumin, a novel agent extracted from Curcuma longa (turmeric), has attracted extensive attention from scientists due to its high therapeutic potential. Recent in vivo and in vitro studies have demonstrated the antineoplastic activities of curcumin [45–50]. In NPC, curcumin has been found to attenuate carcinogenesis by suppressing cell proliferation, inducing cell apoptosis, and enhancing the radiotherapy response [51–53]. Furthermore, significant synergistic activity of curcumin in combination with chemotherapy drugs, including 5-FU, has been documented to address drug resistance in head and neck squamous carcinoma, colorectal cancer, and breast cancer cells [54–56]. These findings suggest that curcumin may also have potential as an adjunctive chemotherapy in treating NPC patients.

In this study, we investigate 5-FU chemoresistance in NPC cells and identify an unexpected dependency on a mutant p53 gain-of-function affecting DNA repair machinery. By carrying out RNA-seq and ChIP-seq studies to systematically dissect mutant p53 oncogenic functions, we identify KMT5B as a key molecule involved in p53(R280T)-mediated 5-FU resistance. We also demonstrate that curcumin, a naturally occurring compound that induces KMT5B downregulation, synergistically inhibits NPC tumor growth in combination with 5-FU treatment. Suppression of DNA repair machinery may offer effective salvage or potentially even first-line therapies to overcome mutant p53-induced 5-FU resistance in NPC patients.

2. Results

2.1. p53(R280T) shows impairment of tumor suppressor activity in NPC cell lines

To understand the basis of 5-FU resistance in NPC, we first examined the role of p53 signaling in tumor and non-tumor nasopharyngeal cells. RT-qPCR indicated that 5-FU induces the expression of p53 downstream targets *CDKN1A* and *PUMA* in the immortalized but non-tumorigenic nasopharyngeal epithelial cell line, Np69, but fails to induce this response in multiple NPC lines, including CNE1, CNE2, C666.1, and SUNE1 (Fig. 1A). The results suggested an impairment of functional p53 tumor suppressor activity in NPC. Sanger sequencing of the *TP53* gene locus identified a distinctive missense mutation (*TP53*; c.839G > C, p. R280T) consistently present in the NPC cell lines, while the Np69 and Np460 cell lines exhibited an intact *TP53* gene (Fig. 1B). Interestingly, analyses of the IARC TP53 database and COSMIC database demonstrated that p53(R280T) is a prevalent hot spot p53 mutation (around 10 % of all p53 mutations) in NPC. Analysis of the published human p53-DNA complex X-ray structure suggested that R280 not only participates in DNA's specificity recognition but also is involved in a network of interactions between the phosphate backbone of T11 and the side chains of G11, R273, and D281, suggesting a considerable function of R280 in supporting p53 binding to DNA duplexes (Fig. 1C). Since MDM2-mediated p53 ubiquitination and degradation critically impacts p53 function [11], we investigated if p53(R280T) retains the capacity to be regulated by MDM2. Immunoprecipitation demonstrated a decreased protein-protein interaction between MDM2 and p53(R280T) compared with wild-type p53 (p53(WT)) (Fig. 1D). Consistently, proteolysis assay following co-expression of MDM2 with either p53(WT) or p53(R280T) demonstrated impaired MDM2-mediated degradation of p53(R280T) compared with p53 (Fig. 1E). Consistently, p53(R280T) protein exhibits greater stability compared to p53(WT), as demonstrated by a

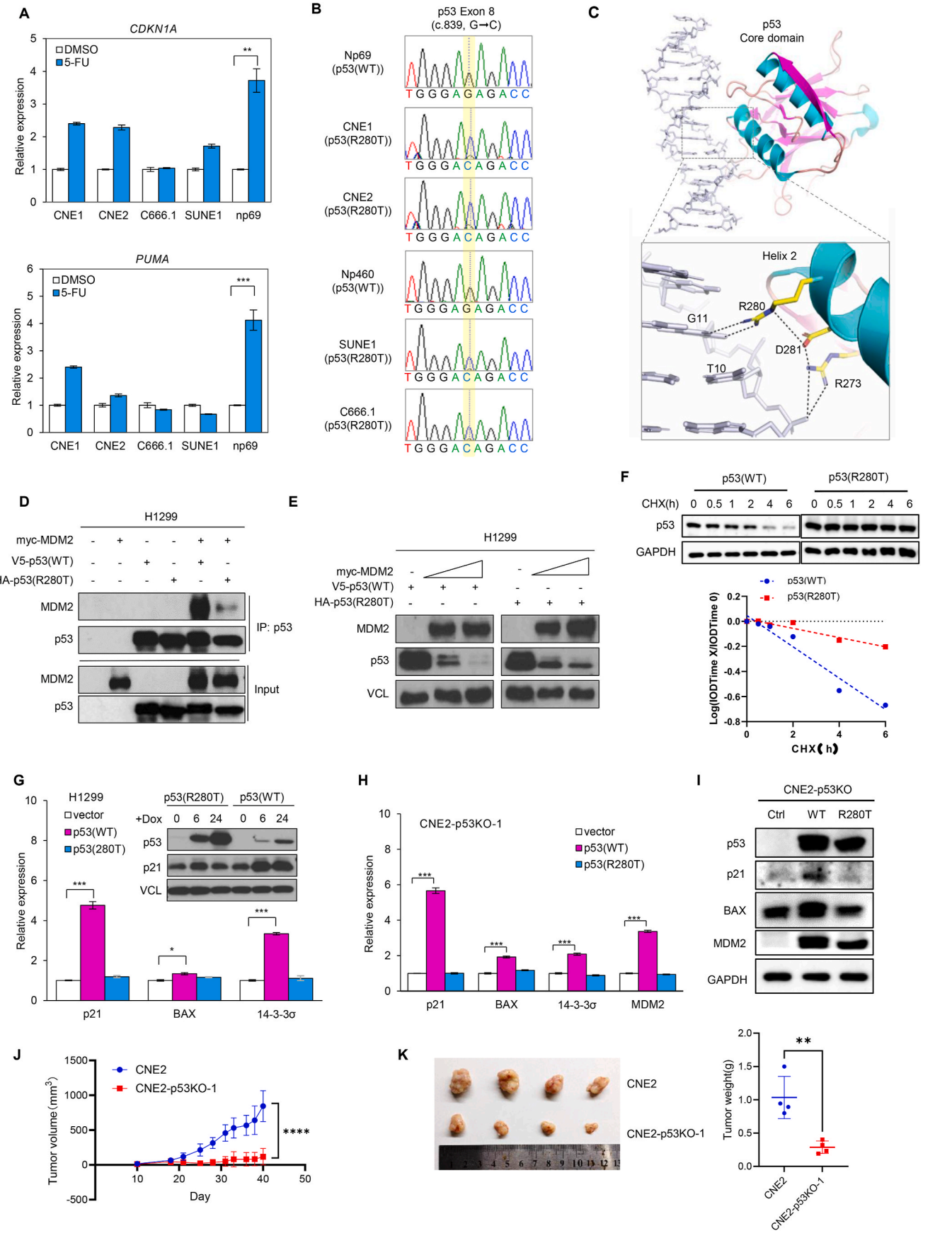

(caption on next page)

Fig. 1. Identification of p53(R280T) mutation and investigation of its role in NPC cells (A) Impairment of 5-FU-induced p53 activation in NPC. RT-qPCR analysis shows the relative levels of p53-regulated CDKN1A and PUMA mRNA in NPC cell lines (CNE1, CNE2, C666.1, and SUNE1) and normal nasopharyngeal epithelial cells (NP69) treated with DMSO or 10 μM 5-FU. CDKN1A and PUMA mRNA levels are normalized to GAPDH mRNA. Data represent the mean ± SEM of three independent experiments. **p < 0.01. (B) Sanger sequencing identifies the p53(R280T) (c.839, G > C) mutation in multiple NPC cell lines, including CNE1, CNE2, SUNE1, and C666.1. (C) Structure and binding mode of the human p53-DNA complex. p53 interacts with DNA nucleotides via residues R273, R280, and D281. DNA and p53 protein are shown as grey sticks and colored ribbons, respectively. The structure is modified from NDB ID: PDR022. (D) Co-immunoprecipitation (Co-IP) reveals that the R280T mutation impairs the interaction between p53(R280T) and MDM2. p53 or p53(R280T) was transfected with MDM2 in H1299 cells, and cell lysates were subjected to Co-IP using an anti-p53 antibody. Input indicates the total lysate used for Co-IP. (E) Immunoblotting shows that the R280T mutation partially impairs MDM2-mediated degradation of p53(R280T). VCL is presented as the internal control. (F) The cycloheximide chase assay demonstrates that p53(WT) has a shorter protein half-life than p53(R280T) when expressed in CNE2-p53KO cells. GAPDH was used as the internal control. (G) RT-qPCR shows that wild-type p53, but not p53 (R280T), induces the upregulation of p53 targets (p21, BAX, and 14-3-3σ) in p53-null H1299 cells. H1299 cells were transfected with tetracycline-inducible wild-type p53 or p53(R280T). Immunoblotting demonstrates the protein expression of p53, p53(R280T), and p21. Data represent the mean ± SD of three independent experiments. *p < 0.05, ***p < 0.001. (H) RT-qPCR shows that wild-type p53, but not p53(R280T), induces the upregulation of p53 targets (p21, BAX, 14-3-3σ, and MDM2) in CNE2-p53KO cells. CNE2-p53KO cells were transfected with tetracycline-inducible wild-type p53 or p53(R280T). Data represent the mean ± SD of three independent experiments. ***p < 0.001. (I) Western blot analysis indicates that p53(R280T) weakly activates p53 targets. CNE2-p53KO cells were transfected with tetracycline-inducible p53(WT) or p53(R280T). Protein expression of p53, p53(R280T), p21, BAX, MDM2, and GAPDH was assessed by immunoblotting, with GAPDH serving as the internal control. (J) Tumor volumes of control and p53-KO groups in a nude mouse xenograft NPC model. n = 4. Data represent the mean ± SD. ****p < 0.0001. (K) Left panel shows representative images of CNE2 cells xenograft tumors in control and p53-KO groups. The right panel shows the tumor weights of indicated groups. Data represent the mean ± SD. *p < 0.05.

cycloheximide chase assay (Fig. 1F). These results indicated that the substitution of positively charged arginine (R) with uncharged threonine (T) likely disrupts p53 protein structure, impairs its interaction with MDM2, and hinders MDM2-mediated proteolysis, leading to a loss of tumor suppressor function and a gain of oncogenic activity.

We subsequently established p53(R280T)-depleted CNE2 cells (CNE2-p53KO) and control CNE2 cells as a functional cell model for studying p53(R280T). The p53 knock-out was generated using two sgRNAs targeting p53 Exon 2 and Exon 4, respectively (Fig. S1A). p53 (R280T) knockout efficiency was validated by immunoblotting confirming no detectable p53(R280T) protein expression in CNE2-p53KO cells (Fig. S1B). In agreement with genotype, RT-qPCR and Western blot analyses showed that, compared to p53(WT), p53(R280T) exhibits impaired transcriptional activation of several known p53 target genes, including *p21*, *BAX*, *14-3-3σ*, and *MDM2* in both CNE2-p53KO and p53-null H1299 cells (Fig. 1G, H, and 1I). Furthermore, in vivo xenograft experiments demonstrated reduced tumorigenesis in CNE2-p53KO cells compared to parental CNE2 cells harboring p53(R280T) (Fig. 1J). Both tumor volume and weight were significantly lower in the CNE2-p53KO group than in the CNE2 group (Fig. 1J and K). These findings suggest a potential gain-of-function role for p53(R280T) in NPC development.

2.2. p53(R280T) confers 5-FU resistance in NPC cell lines

Given the potential oncogenic role of p53(R280T) in NPC, we investigated whether p53(R280T) contributes to chemoresistance, particularly resistance to 5-FU, in NPC. Cell proliferation assay revealed increased sensitivity to 5-FU mediated growth inhibition in p53-knockdown CNE2 cells cells compared with CNE2 cells (Fig. 2A). CNE2 cells harboring p53(R280T) exhibited resistance to 5-FU and formed colonies, whereas depletion of p53(R280T) significantly increased 5-FU sensitivity, resulting in minimal colony formation after treatment (Fig. 2B). Consistently, 5-FU resistance was also observed in SUNE1, another NPC cell line harboring p53(R280T), and this chemoresistance was abolished following p53(R280T) knockdown using two distinct shRNAs targeting p53 (shp53-1 and shp53-2) (Fig. 2C and D). Moreover, 5-FU selectively inhibited the in ovo tumorigenic ability of p53-knockdown CNE2 cells but not CNE2 cells in chick chorioallantoic membrane (CAM) assay (Fig. 2E). Taken together, our in vitro and in ovo studies highlight that p53(R280T) confers resistance to 5-FU in NPC.

To explore how 5-FU mediates growth inhibition in NPC, we analyzed cell apoptosis using flow cytometry. We specifically examined the sub-G1 cell population, as these cells, characterized by fractional DNA content, predominantly represent the apoptotic population. 5-FU treatment increased the proportion of sub-G1 cells in CNE2 cells (from 3.61 % to 21.2 % of total cells) and caused an even more pronounced increase in CNE2-p53KO cells (from 2.55 % to 32.7 %) (Fig. 2F). The negative regulatory role of p53(R280T) in 5-FU-induced apoptosis was confirmed in SUNE1 cells with p53(R280T) knockdown (Fig. 2G). Interestingly, the expression of γ-H2AX, a biomarker for DNA double-strand breaks, was significantly elevated following 5-FU treatment in CNE2-p53KO cells, but not in CNE2 cells harboring p53(R280T) (Fig. 2H). These findings demonstrate that p53(R280T) confers gain-of-function activity to promote tumorigenesis by impairing 5-FU-induced apoptosis and the DNA damage response in NPC.

2.3. Genome-wide ChIP-seq study reveals the gain-of-function of p53 (R280T) in NPC

Many cancer-associated mutant p53s not only lack tumor suppressor functions but also possess gain-of-function oncogenic activities not found in p53(WT) [25,57–61]. We hypothesized that the p53(R280T) mutation induces a gain-of-function by promoting transcriptional activation of genes involved in NPC-associated 5-FU resistance. To identify potential transcriptional targets specifically regulated by p53(R280T), we performed chromatin immunoprecipitation followed by next-generation sequencing (ChIP-seq) in CNE2 cells expressing p53 (R280T) and in CNE2-p53KO cells transduced with p53(WT). This approach allowed us to determine and compare the global genome occupancies of p53(R280T) and p53(WT), respectively. The binding patterns of p53 and p53(R280T) to gene-proximal regions (less than 3 kb) near transcription start sites (TSSs) were analyzed. In accordance with our hypothesis, ChIP-seq analyses revealed remarkably little overlap between the genome-wide p53 and p53(R280T) binding regions, which included 67 shared peaks, 700 p53 unique peaks, and 1791 p53(R280T) unique peaks in CNE2 cells (Fig. 3A). These findings indicate that p53 (R280T) not only loses DNA binding to typical p53 transcriptional targets but also binds to a unique set of genomic loci at sites critical for gene expression regulation. Moreover, in comparison to the identified p53 genome binding loci, where only 39.91 % were located within 3 kb of promoter regions, the p53(R280T) genome binding loci predominantly mapped to promoter regions, accounting for 81.96 % (Fig. 3B), suggesting that p53(R280T) mainly modulates gene transcription directly. Known and de novo motif analysis using the HOMER tool revealed that p53 TSS-proximal peaks are most significantly enriched for p53/p63/p73 binding motifs (Fig. 3C); in contrast, the most significantly enriched known motifs among p53(R280T) TSS-proximal peaks shared similarity to ETV4(ETS) and ZNF75D binding motifs (Fig. 3D), indicating that p53(R280T) may collaborate with other transcription factors to bind directly to specific genomic loci. ChIP-seq read peaks also demonstrated that p53(R280T) loses genome binding to the promoter region of known p53 targets (e.g. p21, ZMAT3, and RPS27L) but acquires binding to the promoters of known mutant p53 targets (e.g. MLL1, MLL2, and ARID3B) [23,62] (Fig. 3E). Together, these ChIP-seq

analyses suggest that p53(R280T) abolishes certain p53(WT) functions while enabling regulation of new categories of gene expression in CNE2 cells.

Gene Ontology Biological Process (GO_BP) analysis of p53(R280T)-bound proximal gene regions revealed a distinct enrichment of DNA repair-related processes, such as DNA repair and global genome nucleotide-excision repair (Fig. 4A). This contrasts with the enrichment of p53-specific targets, which are primarily associated with processes like signal transduction involved in mitotic G1 DNA damage checkpoint and cell cycle regulation (Fig. 4A). The enrichment of p53(R280T) specific binding targets in DNA damage-related pathways (e.g. ATM pathway, nucleotide excision repair, DNA repair, DSBs and cellular response via ATM, and DNA IR-damage and cellular response via ATR) was also observed in the BioPlanet and Wikipathway analyses (Fig. S2A and S2B). Metascape GO analysis also supported that p53(R280T)-specific binding targets are enriched in DNA repair and regulation of

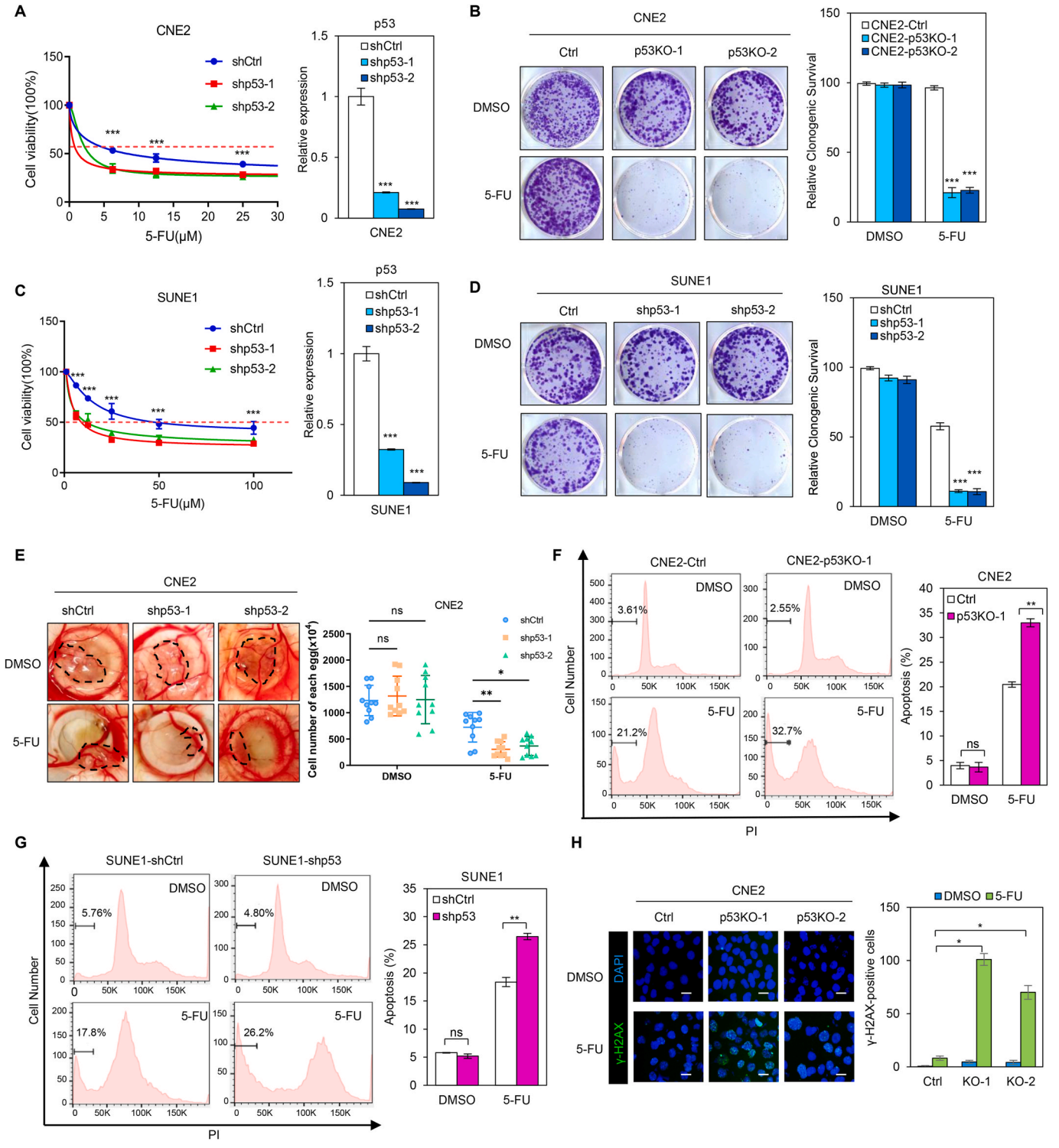

(caption on next page)

Fig. 2. p53(R280T) mutation confer 5-FU resistance in NPC cells (A) Depletion of p53(R280T) selectively inhibits the proliferation of 5-FU-treated CNE2 cells. (Left panel) An MTT assay evaluates the viability of CNE2 and p53(R280T)-depleted CNE2 cells following 5-FU treatment. (Right panel) RT-qPCR confirms the knockdown efficiency of p53(R280T). Data are presented as the mean ± SD/SEM from three independent experiments. ***$p < 0.001$. (B) Colony formation assay reveals that p53 (R280T) depletion reduces 5-FU resistance in CNE2 cells. CNE2-Ctrl and CNE2-p53KO cells are treated with DMSO or 5 μM 5-FU for 3 days and subsequently cultured in normal medium for 1 week. Colonies are stained with crystal violet and quantified using a microplate reader at OD595. Results represent three biological replicates; error bars indicate ±SD. Statistical significance is determined by two-way ANOVA; ***$p < 0.001$. (C) Knockdown of p53(R280T) selectively reduces the proliferation of 5-FU-treated SUNE1 cells. (Left panel) An MTT assay evaluates the viability of SUNE1 and p53(R280T)-depleted SUNE1 cells following 5-FU treatment. (Right panel) RT-qPCR confirms the knockdown efficiency of p53(R280T). Data are presented as the mean ± SD from three independent experiments. ***$p < 0.001$. (D) Colony formation assay demonstrates that p53(R280T) depletion diminishes 5-FU resistance in SUNE1 cells. SUNE1-shCtrl and SUNE1-shp53 cells are treated with DMSO or 4 μM 5-FU for 3 days and subsequently cultured in normal medium for 1 week. Colonies are stained with crystal violet and quantified using a microplate reader at OD595. Results represent three biological replicates; error bars indicate ±SD. Statistical significance is determined by two-way ANOVA; ***$p < 0.001$. (E) In ovo CAM assay demonstrates that p53(R280T) depletion enhances 5-FU-mediated inhibition of tumorigenesis in CNE2 cells. One and a half million cells were implanted for the tumorigenesis assay. Data are presented as the mean ± SD from independent experiments. **$p < 0.01$, ***$p < 0.001$. (F) Flow cytometry analysis of cell cycle distribution shows that p53KO increases the sub-G1 phase in CNE2 cells upon 5-FU treatment. CNE2-Ctrl and CNE2-p53KO cells are treated with 30 μM 5-FU for 48 h, stained with PI, and analyzed by flow cytometry. Histograms show an increased sub-G1 phase in CNE2-p53KO cells compared with CNE2-Ctrl cells. Data are presented as the mean ± SD from three independent experiments. **$p < 0.01$. (G) Flow cytometry analysis of cell cycle distribution shows that p53 knockdown increases the sub-G1 phase in SUNE1 cells upon 5-FU treatment. SUNE1-shCtrl and SUNE1-shp53 cells are treated with 30 μM 5-FU for 48 h, stained with PI, and analyzed by flow cytometry. Histograms show an increased sub-G1 phase in SUNE1-shp53 cells compared with SUNE1-shCtrl cells. Data are presented as the mean ± SD from three independent experiments. **$p < 0.01$. (H) γ-H2AX immunofluorescence staining shows 5-FU-induced DNA damage in CNE2-Ctrl and CNE2-p53KO cells. Nuclei are stained with DAPI. Quantitative analysis of positive cells is performed using ImageJ. Data are presented as the mean ± SD from three independent experiments. *$p < 0.05$. Scale bar, 10 μm.

response to DNA damage stimulus pathways (Fig. 4B). Furthermore, protein-protein interaction (PPI) analysis identified that p53(R280T)-specific ChIP targets corresponded to DNA repair process proteins (Fig. 4C, left panel), while p53-specific ChIP targets and shared targets corresponded to cellular response to stress and DNA damage response processes, respectively (Fig. 4C, middle and right panels). Gene Set Enrichment Analysis (GSEA) of transcripts in NPC and normal nasopharyngeal mucosa tissues revealed the enrichment of p53(R280T)-specific binding genes in NPC (Fig. 4D), suggesting an oncogenic ability of the predominant p53(R280T) mutation in driving a transcriptional signature in NPC.

To examine if p53(R280T) shares genomic target similarity with other gain-of-function mutant p53s (p53(R248Q), p53(R249S), and p53 (R273H)), we compared ChIP-seq results among each p53 mutant. We found that p53(R280T) genomic binding peaks largely differ from other hot-spot mutant p53s genomic binding peaks (Fig. 4E–G), although some targets (e.g., MLL1 and MLL2) were shared among distinct mutant p53s (Fig. 3E) [23]. Together, these results suggest that p53(R280T) plays a critical and unique gain-of-function role in regulating DNA repair, which may contribute to 5-FU resistance in NPC.

2.4. p53(R280T) transcriptionally upregulates DNA repair-associated genes KMT5B and CCNG2 in NPC

An analysis of transcriptomic alterations following exposure to various chemotherapies and other compounds with potential therapeutic roles in multiple cancers revealed that 5-FU most consistently and dramatically downregulated p53(R280T) genome-bound targets among the panel of 36 drugs (Fig. 5A). Treatments for locally advanced and recurrent NPC routinely include 5-FU as a first-line therapy; however, its effectiveness is often limited by the development of chemo-resistance. Given that 5-FU downregulates p53(R280T) targets, it is likely that p53(R280T)-mediated transcripts play a role in the development of 5-FU resistance in NPC. To dissect the fundamental mechanisms underlying 5-FU resistance driven by p53(R280T), we investigated and compared the global transcriptomes of CNE2-Ctrl and CNE2-p53KO cells. RNA from CNE2-Ctrl and CNE2-p53KO lines was isolated and analyzed by RNA-seq. A heatmap of RNA-Seq expression, computed using z-scores, revealed significant differences between the transcriptomes of CNE2-Ctrl and CNE2-p53KO cells (Fig. 5B). Differentially expressed genes (DEG) between CNE2-Ctrl and CNE2-p53KO cells were further analyzed and presented in a volcano plot. Compared to CNE2-Ctrl cells, CNE2-p53KO cells exhibited significant downregulation of numerous known NRF2 pathway targets (e.g., GPX2 and TXNRD3), fatty acid biosynthesis genes (e.g., SCD and ACACB), DNA repair-associated factors (e.g., KMT5B, CCNG2, SWSAP1, and DICER1), and cancer stem cell genes (e.g., SOX2). Concurrently, CNE2-p53KO cells showed upregulation of genes involved in rRNA processing and ribosome biogenesis (e.g., RRP12, POP4, NOLC1, and WDR46) (Fig. 5C). GO_BP analyses of these DEGs between CNE2-Ctrl and CNE2-p53KO cells indicated that p53 (R280T) upregulates genes involved in metabolic processes, oxygen transport, regulation of cell cycle arrest, and signal transduction in response to DNA damage but downregulates genes involved in cell migration and adhesion, regulation of MAPK pathway and cytokine-mediated signaling (Fig. 5D).

By integrating RNA-seq and ChIP-seq data, we identified 51 genes transcriptionally regulated by p53(R280T) via direct genome binding to the promoter/TSS region (Fig. 5E). Since 5-FU treatment has been shown to induce DNA damage responses [63], we hypothesized that the upregulation of DNA repair genes conferred 5-FU resistance in NPC. Indeed, multiple signaling molecules known to be involved in DNA repair, including CCNG2 [64], KMT5B [65,66], SWSAP1 [67,68], and DICER1 [69], were among the 51 p53(R280T) transcriptionally regulated genes (Fig. 5F and Fig. S3A). ChIP-seq peak analysis demonstrated binding of p53(R280T) but not p53 to the promoters/TSS of CCNG2 and KMT5B (Fig. 5F and Fig. S3A). Other mutant p53s, namely p53(R248Q), p53(R249S), and p53(R273H), did not bind to the proximal promoter/TSS of *CCNG2*, *KMT5B*, *SWSAP1*, or *DICER1* (Fig. S3B). ChIP-qPCR further validated specific p53(R280T) binding to the promoter regions of CCNG2 and KMT5B and lack of binding to the same region by p53 (Fig. 5G). RT-qPCR validated the lower *CCNG2* and *KMT5B* mRNA expression in CNE2-p53KO cells compared with CNE2-Ctrl cells (Fig. 5H). The reduced mRNA expression of CCNG2 and KMT5B observed in CNE2-p53KO cells upon the elimination of p53(R280T) was restored by reintroducing p53(R280T) (Fig. 5I and Fig. S3C). Together, these results highlight the transcriptional regulatory role of p53(R280T) in activating the DNA repair machinery, potentially contributing to 5-FU resistance in NPC.

2.5. p53(R280T)-induced KMT5B confers 5-FU resistance in NPC cells

Given that the primary therapeutic effect of 5-FU occurs through induction of DNA damage, especially double- or single-stranded breaks [63], we sought to investigate whether KMT5B, a p53(R280T)-regulated DNA damage repair gene, contributes to 5-FU resistance in NPC cells. KMT5B, also known as SUV4-20H1, is a histone-lysine N-methyltransferase required for proper DNA damage repair. It deposits H4K20 methyl marks to damaged DNA to enable 53BP1 binding [65,66]. Immunofluorescence (IF) staining revealed a significant increase of γ-H2AX signal and γ-H2AX positive cells following 5-FU treatment in

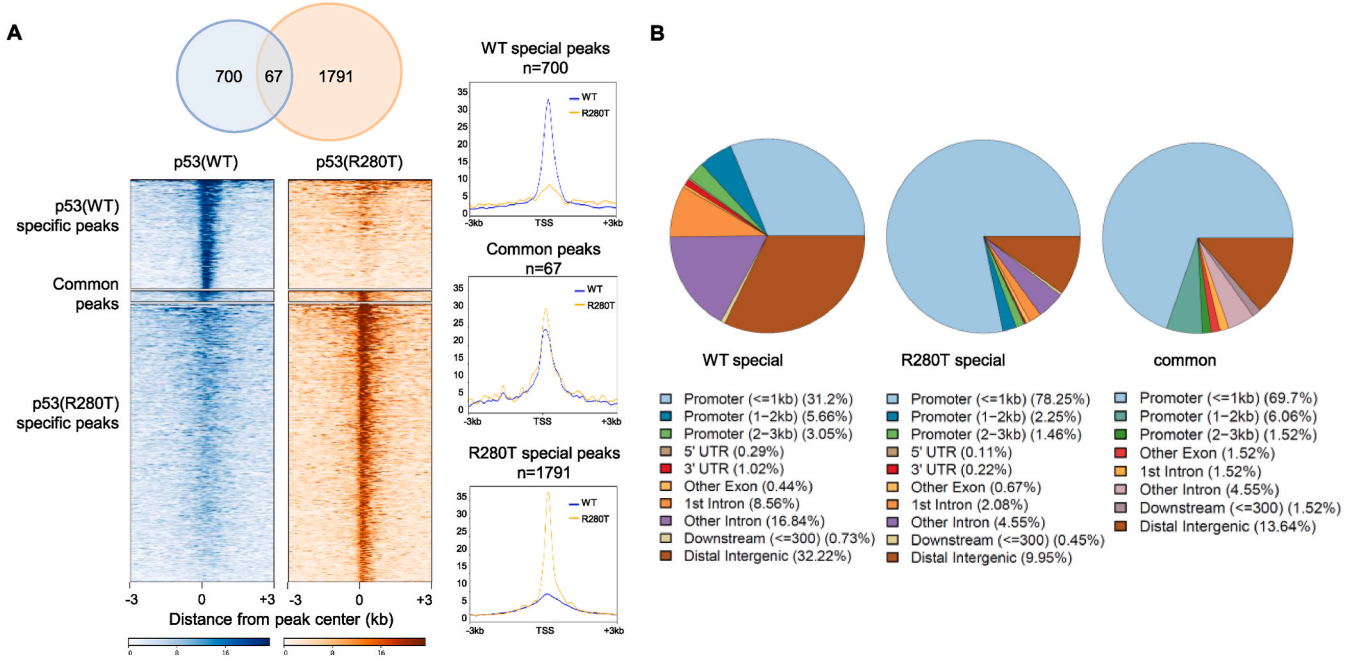

C

Homer Known Motif Enrichment

WT	p-value	TF
	1e-568	p73(p53)
	1e-505	p53
	1e-291	p63(p53)
	1e-44	ZNF416(Zf)

Homer *de novo* Motif Enrichment

WT	p-value	TF
TGTCTTAGGCAA	1e-86	HLF
ATAAGAAAGGGT	1e-82	Foxa2
GCTCTTAGCTTG	1e-76	Nr2e3
TATGGAGTAACT	1e-69	Obox5

D

Homer Known Motif Enrichment

R280T special	p-value	TF
	1e-13	ETV4(ETS)
	1e-10	Elk4(ETS)
	1e-6	Fos(bZIP)
	1e-4	CTCF(Zf)

Homer *de novo* Motif Enrichment

R280T special	p-value	TF
GTCAGTCCCACC	1e-30	ZNF75D
GTTTTTTAAGCC	1e-21	FoxD3
ATACTGCGGCTTT	1e-21	Hnf4a
TTAGCTAAGCAA	1e-19	DBP

E

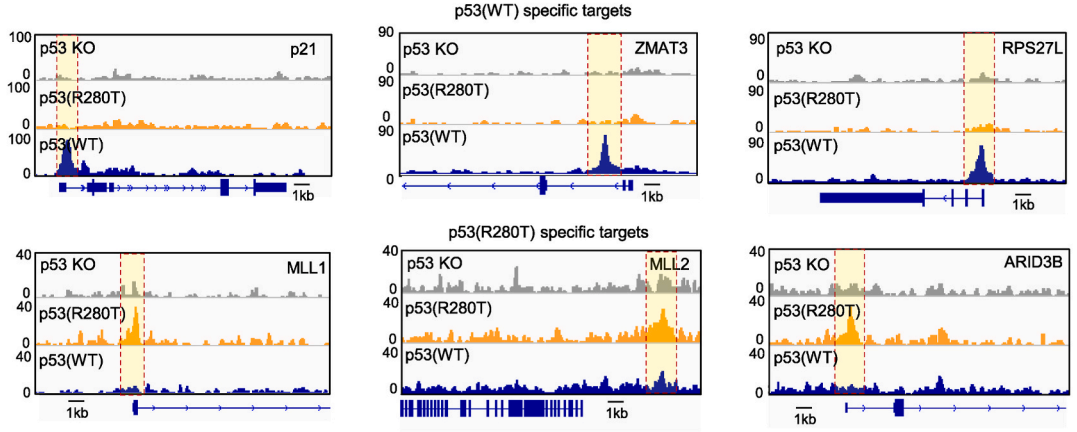

(caption on next page)

Fig. 3. ChIP analysis of p53 and p53(R280T) genome occupancies in NPC cells (A) (Top left) The Venn diagram illustrates the overlap between p53 and p53(R280T) binding peaks in CNE2 cells. ChIP-seq analysis identifies 700 p53-specific, 1791 p53(R280T)-specific, and 67 common promoter/TSS genomic binding sites. (Bottom left) A heatmap shows p53 and p53(R280T) binding across the 3 kb genomic regions surrounding the ChIP-seq peaks. (Right) Composite plots present average binding signals for p53-specific, p53(R280T)-specific, and common p53/p53(R280T) peaks. (B) Pie charts depict the genomic distribution annotations of p53-specific, p53(R280T)-specific, and common p53/p53(R280T)-targeted genomic binding sites in relation to known RefSeq genes. (C) HOMER motif analysis of wild-type p53 genomic binding peaks in CNE2 cells reveals the top-scoring motifs for known (Top) and de novo (Bottom) binding sites. (D) HOMER motif analysis of p53(R280T) genomic binding peaks in CNE2 cells identifies the top-scoring motifs for known (Top) and de novo (Bottom) binding sites. (E) IGV browser views illustrate p53-KO (p53-null), p53, and p53(R280T) occupancy at promoter regions of representative p53(WT)-target genes (e.g., p21, ZMAT3, and RPS27L) (Top) as well as mutant p53-specific target genes (e.g., MLL1, MLL2, and ARID3B) (Bottom).

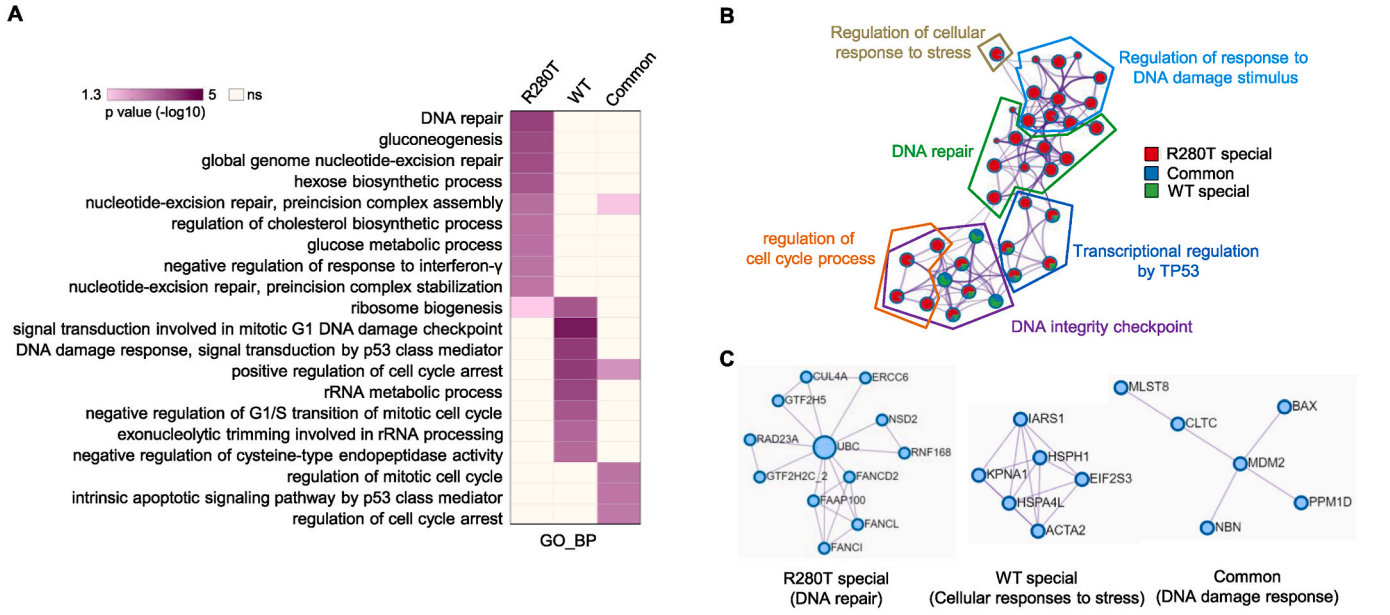

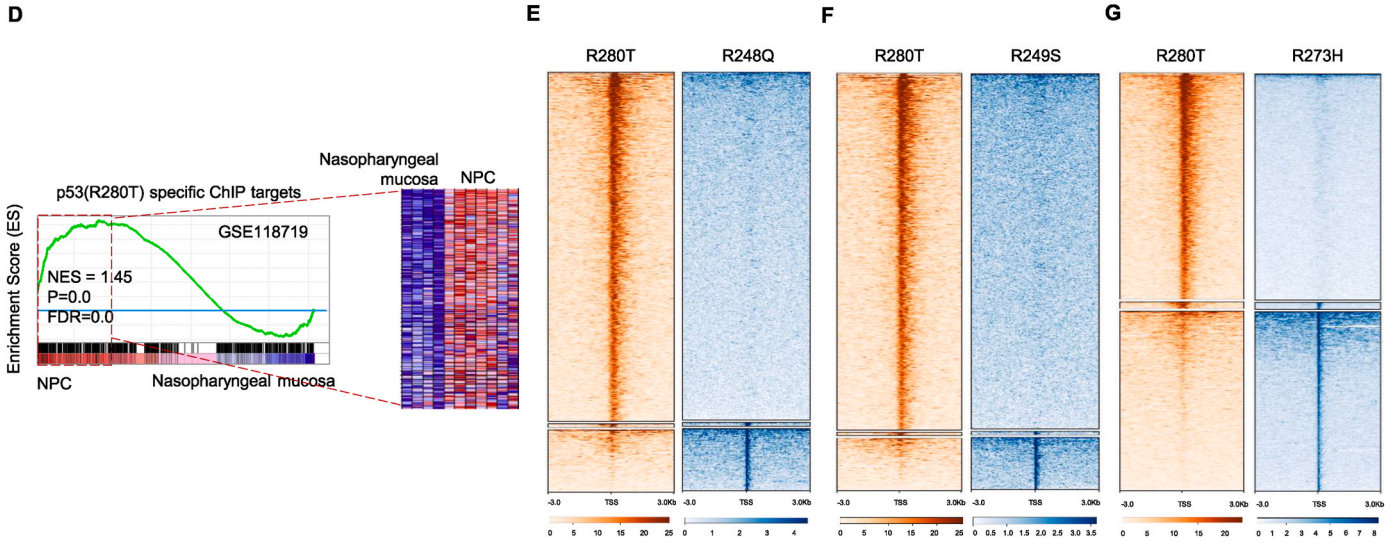

Fig. 4. Gain-of-function role of p53(R280T) in regulating DNA repair and mediating 5-FU resistance in NPC (A) GO_BP analysis using Enrichr highlights the unique enrichment of DNA repair processes, global genome nucleotide-excision repair, and nucleotide-excision repair preincision complex assembly-related genes specifically in p53(R280T) genomic targets. (B) Biological processes and pathways enriched in p53, p53(R280T), and common p53/p53(R280T) genomic targets are analyzed and visualized as a network using Metascape. Enriched pathways and processes are color-coded: green for p53, red for p53(R280T), and blue for shared p53/p53(R280T) targets. (C) Network visualization of protein-protein interactions (PPI) among biological processes associated with p53(R280T) targets, as identified by Metascape analysis. (D) Gene Set Enrichment Analysis (GSEA) reveals significant enrichment of p53(R280T)-specific targets in NPC cells compared to nasopharyngeal mucosa. (E–G) Heatmap clustering of unique and shared genomic binding peaks compares p53(R280T) with other p53 mutants: p53(R248Q) (E), p53 (R249S) (F), and p53(R273H) (G).

KMT5B-depleted CNE2 and SUNE1 cells (Fig. 6A and S4A), indicating the essential inhibitory role of KMT5B in the response of 5-FU-induced DNA damage in NPC. The knockdown of KMT5B sensitized the 5-FU response in NPC and led to lower colony formation in KMT5B-depleted CNE2 and SUNE1 cells compared to control CNE2 and SUNE1 cells (Fig. 6B and S4B). Caspase 3/7 activity assays indicated that depletion of KMT5B led to increased cell apoptosis in 5-FU-treated CNE2 cells (Fig. 6C). These findings suggest that KMT5B plays a crucial role in p53(R280T)-mediated 5-FU resistance in NPC.

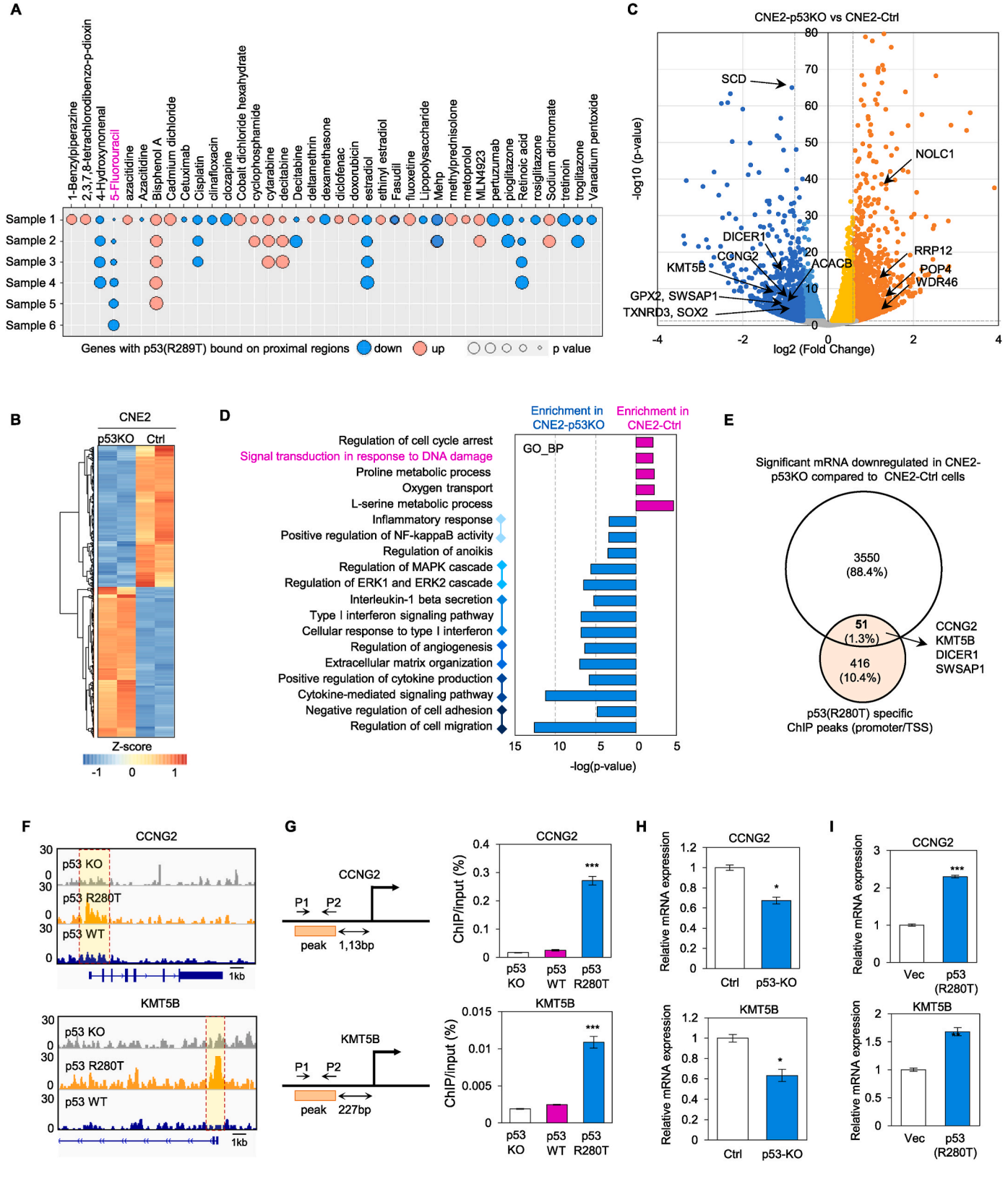

(caption on next page)

Fig. 5. p53(R280T) transcriptionally upregulates DNA damage repair genes in NPC (A) Enrichr analysis of p53(R280T) ChIP targets reveals transcript upregulation (red) and/or downregulation (blue) following treatment with distinct chemotherapeutic compounds. (B) Heatmap depicting significant transcript differences between CNE2-Ctrl and CNE2-p53KO cells, computed using z-scores. (C) Volcano plot illustrating differential gene expression between CNE2-Ctrl and CNE2-p53KO cells. Significantly upregulated genes upon p53(R280T) knockout are shown in orange (fold change ≥2) and yellow (fold change <2), while significantly downregulated genes are depicted in dark blue (fold change ≥2) and blue (fold change <2). Insignificant transcripts ($p > 0.05$) are presented in grey. (D) GO_BP pathway analysis of DEGs between CNE2-Ctrl and CNE2-p53KO cells identifies representative pathways. Significant GO_BP pathways are selected based on p and q values < 0.05. (E) Venn diagram showing overlap between p53(R280T)-specific genomic targets and downregulated transcripts in CNE2-p53KO cells relative to CNE2-Ctrl cells. A total of 51 transcripts, including DNA repair genes CCNG2, KMT5B, SWAP1, and DICER1, were identified. (F) IGV snapshot highlighting p53(R280T) genomic occupancy at the promoter/TSS regions of CCNG2 and KMT5B. (G) Left: Schematic representation of the amplicon locations for CCNG2 and KMT5B ChIP-qPCR validation. Right: ChIP-qPCR confirms p53(R280T) binding peaks at the promoter/TSS regions of CCNG2 and KMT5B in CNE2 cells. Data represent the mean ± SD of three independent experiments. ***$p < 0.001$. (H) RT-qPCR analysis shows downregulation of CCNG2 and KMT5B in CNE2-p53KO cells compared to CNE2-Ctrl cells. Data represent the mean ± SD of three independent experiments. *$p < 0.05$. (I) RT-qPCR demonstrates that p53(R280T) restores CCNG2 and KMT5B expression in CNE2-p53KO cells. Data represent the mean ± SD of three independent experiments. **$p < 0.01$, ***$p < 0.001$.

2.6. Curcumin sensitizes NPC to 5-FU therapy by repressing KMT5B

Given the critical role of KMT5B expression in 5-FU resistance, we screened compounds that can downregulate KMT5B, as they may have therapeutic potential in sensitizing NPC to 5-FU therapy. We preselected 26 potential compounds used or investigated for cancer treatment to assess their effects on KMT5B expression and found that curcumin, rotenone, and perampanel effectively suppress KMT5B expression in NPCs (Fig. 6D). Among them, curcumin was selected for future investigation due to its anti-inflammatory properties and availability as a dietary supplement, making it a potential option for continuous supplementation in NPC patients after chemotherapy. Treatment of CNE2 and SUNE1 cells with curcumin significantly reduced the expression of both p53(R280T) and KMT5B (Fig. 6E and Fig. S4C), supporting the notion that curcumin suppresses p53(R280T), thereby leading to decreased KMT5B expression. Consistently with this observation, the ectopic expression of p53(R280T), but not p53(WT), activated KMT5B expression (Fig. 6F). Taken together, our findings suggest that curcumin downregulates KMT5B by inhibiting p53(R280T) expression.

5-FU and curcumin combination treatment markedly decreased cell viability compared with 5-FU or curcumin treatment alone (Fig. 6G, left panel, and Fig. S4D, left panel), consistent with the reported synergistic effects of curcumin with other chemotherapies [65,66]. In CNE2 and SUNE1 cells, cotreatment with 2.5 μM curcumin reduced cell viability following 5-FU treatment across a range of 5-FU doses (1.25–10 μM) (Fig. 6G, middle panel, and S4D, middle panel). The Combination Index (CI) [70,71], which reflects the degree of synergy between curcumin and 5-FU across the tested range of 5-FU doses, demonstrated a synergistic effect (CI value < 1) with addition of curcumin in CNE2 cells (5-FU [2.5–10 μM]) but also in SUNE1 cells (5-FU [2.5–10 μM]) (Fig. 6G, right panel, and S4D, right panel, and Table 1). The colony forming assay further supported the synergistic effect of curcumin in 5-FU treated NPC (Fig. 6H). In ovo CAM assay demonstrated a significant reduction in cell numbers within NPC tumors following concurrent treatment of curcumin and 5-FU, compared to treatment with 5-FU alone. (Fig. 6I). The xenograft study also showed that the volume and weight of NPC tumors were decreased in the groups treated with curcumin, 5-FU, or both curcumin and 5-FU, compared to the control group (Fig. 6J and K). Importantly, the therapeutic efficacy of 5-FU was enhanced by curcumin, as the combination treatment more effectively inhibited tumor growth, functionally confirming the synergistic effect. In summary, these results suggest that inhibition of KMT5B by curcumin improves the efficacy of 5-FU treatment in 5-FU-resistant NPC with p53(R280T).

3. Discussion

The majority of p53 mutations found in cancers are missense mutations in the DNA binding domain. While each amino acid substitution has the potential to alter p53 structure, DNA binding, and interactions with partner proteins, certain p53 mutations not only impair tumor suppressor functions but also confer oncogenic properties, including chemotherapy resistance [72–74]. For NPC, the mutation rate of p53 reaches 30 %, and R280T is one of the hotspot mutant sites [75]. In NPC cells, Li J et al. demonstrated that p53(R280T) exhibits loss-of-function and may misfold to form aggregates with the assistance of Hsp90, which impedes its entry into the nucleus and disrupts the initiation of transcription for downstream target genes [10]. In the current study, we conducted a multiomics analysis combining ChIP-seq and RNA-seq to investigate the gain-of-function properties of p53(R280T) and identify p53(R280T)-modulated transcripts. Our systems approach provides mechanistic insights into p53(R280T)-associated 5-FU resistance in NPC patients. We identified that p53(R280T) transcriptionally regulates a set of molecules involved in DNA damage repair, including CCNG2, KMT5B, SWSAP1, and DICER1. Mechanistic and functional analyses revealed that mutant p53, particularly p53(R280T), can hijack the epigenome network by transcriptionally upregulating the histone methyltransferase KMT5B, leading to 5-FU resistance. Interestingly, previous studies have shown that other mutant p53 variants, such as p53(R248Q), p53(R249S), and p53(R273H), can upregulate histone methyltransferases MLL1 and MLL2 [23], and mutant p53 variants such as p53(R175H) and p53(G245D) can form novel transcriptional complexes and recruit MLL1 to promote an open-chromatin structure and facilitate gene transcription [25]. These findings underscore the hijacking of the epigenome as a common gain-of-function mechanism contributing to the oncogenic properties of mutant p53.

5-FU has been widely used for clinical treatment of various cancers, including NPC [76]. However, the efficacy of 5-FU-based chemotherapy has been clinically limited due to chemo-resistance and dose-limiting cytotoxicity [77]. Understanding the mechanisms of 5-FU resistance in NPC is an essential step toward overcoming resistance and improving NPC patients' overall survival. p53 mutations are detected in more than half of human cancers, many of which play an important role in 5-FU resistance [78,79]. However, this study is the first to establish the pathological mechanisms of mutant p53 gain-of-function in 5-FU resistant NPC, providing important insights into overcoming NPC chemoresistance. Since targeting the mutant p53-dependent signaling network can be an effective approach for treatment [80], we performed the screening based on the regulation of KMT5B. Interestingly, curcumin, a natural compound identified in our screening for chemicals downregulating KMT5B in NPCs, has been demonstrated to sensitize multiple cancers (including osteosarcoma, fibrosarcoma, breast, lung, cervical and colorectal cancer) to chemotherapeutic drugs via induction of DNA damage and modulation of DNA repair of double-strand breaks [56,81,82]. The minimal toxicity of curcumin underscores its potential as a component of combination cancer chemotherapy [83]. Our finding highlights the potential of combining curcumin with 5-FU for the treatment of 5-FU-resistant NPC. Since p53(R280T) induces oncogenic gain-of-function in several tumor types, including bladder [84], glioma [85], and nasopharynx, we speculate that similar combined treatments downregulating KMT5B may enable effective chemotherapy targeted against mutant p53(R280T) that continues to effectively activate the p53 DNA damage response.

ChIP analysis in NPC cells demonstrated that p53(R280T) genomic

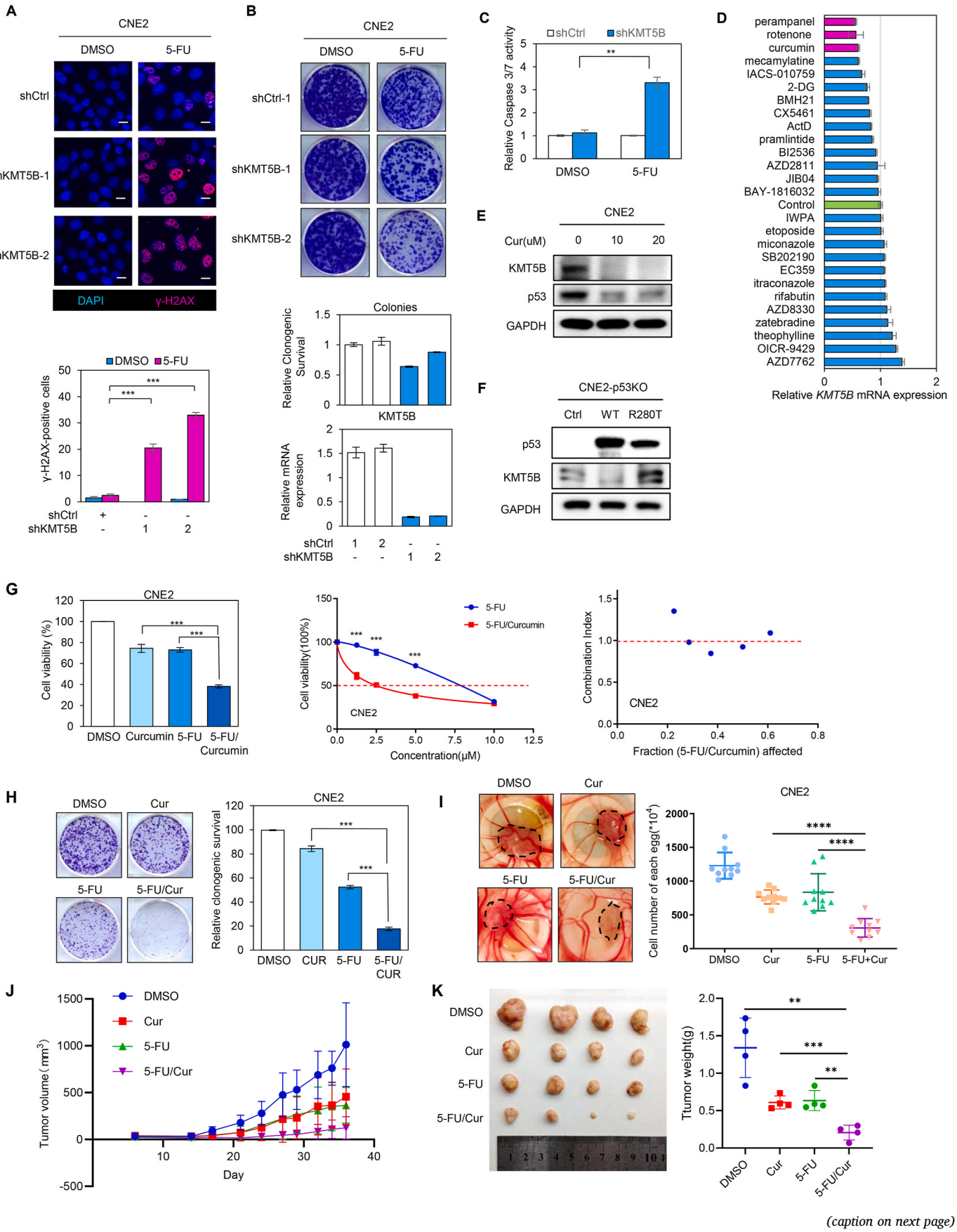

(caption on next page)

Fig. 6. Curcumin synergistically enables 5-FU therapy by inhibiting p53(R280T)-upregulated KMT5B in NPC (A) IF staining shows that knockdown of KMT5B leads to a significant increase in γ-H2AX in 5-FU-treated CNE2 cells. Nuclei were stained with DAPI. Quantitative positive cells were analyzed using ImageJ. Data represent the mean ± SD of three independent experiments. *$p < 0.05$. Scale bar: 10 μm. (B) Colony-forming assay of KMT5B-depleted CNE2 cells in response to 5-FU treatment demonstrates that knockdown of KMT5B reduces 5-FU resistance in CNE2 cells. CNE2-shCtrl and CNE2-shKMT5B cells were treated with DMSO or 5 μM 5-FU for 3 days and then grown in normal culture medium for an additional week. Surviving colonies were stained with crystal violet and quantified by a microplate reader at OD595. n = 3 biological replicates; error bars represent ±SD; statistical significance was determined using two-way ANOVA; ***$p < 0.001$. (C) Cell apoptosis assay measures Caspase 3/7 activities upon 5-FU treatment in CNE2-shCtrl and CNE2-shKMT5B cells. Data represent the mean ± SD of three independent experiments. **$p < 0.01$. (D) Drug screening identifies compounds capable of downregulating KMT5B mRNA expression. Data represent the mean ± SD of three independent experiments. **$p < 0.01$. (E) Immunoblotting reveals the decrease of p53(R280T) and KMT5B protein levels in response to curcumin treatment in CNE2 cells. GAPDH serves as an internal control. (F) Immunoblotting indicates that ectopic expression of p53(R280T) upregulates KMT5B protein levels, while p53 (WT) suppresses KMT5B expression. GAPDH serves as an internal control. (G) Cell viability assay shows the in vitro synergistic effect of combining 5-FU and curcumin to inhibit CNE2 cell growth. (Left panel) The cell viability of CNE2 cells treated with 5-FU, curcumin, and the combination of 5-FU/curcumin was measured by MTT assay. (Middle panel) The cell viability of CNE2 cells treated with individual 5-FU or the combination treatment with 2.5 μM curcumin for 3 days is shown. The cell viability curve indicates that the combination treatment of 5-FU and curcumin significantly inhibits CNE2 cell proliferation and survival. (Right panel) CI values demonstrate that curcumin has a synergistic effect with 5-FU (CI < 1). CI values were calculated based on the quantification of cell viability in CNE2 cells treated with 5-FU combined with curcumin and single 5-FU. Data are presented as mean ± SD for three independent replicates. CI < 1 indicates synergism, CI = 1 indicates additivity, and CI > 1 indicates antagonism. ***$p < 0.001$. (H) Colony-forming assay reveals the synergistic effect of curcumin and 5-FU in suppressing CNE2 colony formation. CNE2 cells were treated individually with 4 μM 5-FU, 4 μM curcumin, or 4 μM 5-FU/curcumin for 3 days and then grown in normal culture medium for an additional week. Surviving colonies were stained with crystal violet and quantified by microplate reader at OD595. n = 3 biological replicates; error bars represent ±SD; statistical significance was determined using two-way ANOVA; ***$p < 0.001$. (I) In ovo CAM assay demonstrates the synergistic effect of curcumin and 5-FU in suppressing CNE2 tumorigenesis. Four million cells were implanted for drug treatment. Data represent the mean ± SD of five independent experiments. **$p < 0.01$, ***$p < 0.001$. (J) Tumor volumes in a nude mouse xenograft NPC model treated with control, curcumin, 5-FU, and combination treatment. Data represent the mean ± SD (n = 4). Statistical significance: P(ctrl vs cur) = 0.0781, P(ctrl vs 5-FU) = 0.0271, P(5-FU vs comb) = 0.0798, P(cur vs comb) = 0.0899, P(ctrl vs comb) = 0.0018. (K) Left: Representative images of xenograft tumors from CNE2 cells in control, curcumin, 5-FU, and combination treatment groups. Right: Tumor weights in the indicated groups. Data represent the mean ± SD. *$p < 0.05$, **$p < 0.01$, ***$p < 0.001$.

Table 1
5-FU and curcumin synergistically inhibit NPC cells.

CNE2	5-FU	1.25	2.5	5	10	20
	Cur	2.5	2.5	2.5	2.5	2.5
	CI	1.09093	0.92411	0.84664	0.98052	1.35221
SUNE1	5-FU	1.25	2.5	5	10	20
	Cur	2.5	2.5	2.5	2.5	2.5
	CI	0.51544	0.56837	0.80546	0.95577	1.26066

Synergism is defined by CI: <1, Additive Effect with CI = 1; and Antagonism by CI > 1.

occupancy sites and binding motifs are distinct from those of p53, supporting the idea that p53(R280T) may exhibit gain-of-function by regulating novel gene expression. Pathway enrichment analysis revealed that the promoters/TSSs of many DNA repair pathway genes are bound by p53(R280T). Interestingly, motif analysis showed that p53(R280T) binding motifs are familiar to ETV4(ETS) and ZNF75D motifs, implying that p53(R280T) may interact and cooperate with other transcriptional factors and regulators such as these to modulate chromatin remodeling and gene expression. Furthermore, a comparison of the genome binding sites of p53(R248Q), p53(R249S), p53(R273H), and p53(R280T) revealed that p53(R280T) has distinct binding capabilities, differing from those of p53(R248Q), p53(R249S), and p53(R273H). Many promoter/TSS regions of DNA repair genes (e.g., CCNG2, KMT5B, SWSAP1, and DICER1) were uniquely bound by p53(R280T), but not by p53 (R248Q), p53(R249S), or p53(R273H). These findings highlight the importance of defining the discrete oncogenic functions of mutant p53s in developing personalized therapies. In the future, the characterization of the genomic binding and gene regulation of particular mutant p53s in connection with a particular cancer may be extended to include the assessment of unique chromatin architecture, transcription factors, and epigenomic factors.

In summary, our work demonstrates that p53(R280T) not only disrupts p53 tumor suppressor functions but also directly drives the transcriptional regulation of DNA repair pathways, enabling 5-FU resistance in NPC cells. Targeting the downstream signaling driven by p53(R280T), particularly by blocking KMT5B activation, offers a promising strategy to overcome 5-FU resistance and holds significant potential for clinical NPC treatment.

4. Materials and methods

4.1. Antibodies, chemicals, plasmids, shRNAs, sgRNAs, and primers

Anti-p53 (DO-1, sc-126) antibody was purchased from Santa Cruz Biotechnology and used at 1:1000 for immunoblotting; 8 μL (1.6 μg) was used for co-immunoprecipitation (Co-IP), and 10 μg of sc-126x was used for ChIP-seq. Antibodies against MDM2 (sc-13161, 1:1000 for immunoblotting) and VCL (sc-73614, 1:1000 for immunoblotting) were also obtained from Santa Cruz Biotechnology. The anti-p21 antibody (cat# 2947S, 1:1000 for immunoblotting) was purchased from Cell Signaling Technology. Anti-Bax antibody (610983, 1:1000 for Immunoblotting) was purchased from BD Transduction Laboratories. Anti-GAPDH antibody (60004-1-Ig, 1:4000 for Immunoblotting) was purchased from Proteintech. Anti-KMT5B antibody (TA377881S, 1:1000 for Immunoblotting) was purchased from Origene. HRP-conjugated secondary antibodies (cat# AP130P, 1:3000 for immunoblotting) were obtained from EMD Millipore.

MTT and puromycin were purchased from Research Product International. MG132 (cat# 1748/5) was obtained from R&D Systems. Doxycycline (cat# D9891), 5-Fluorouracil (cat# F6627) and curcumin (cat# C1386) were obtained from Sigma. shRNA, sgRNA and qRT-PCR primers (Supplementary Table 2) were purchased from Integrated DNA Technologies (USA). The shRNA and sgRNA were confirmed by Sanger sequencing in Eton Bioscience Inc and GENEWIZ.

4.2. Cell culture

The poorly differentiated NPC cell lines CNE2 and SUNE1 were generously provided by Professor Chaonan Qian (Sun Yat-sen University Cancer Center, China). HEK-293T and H1299 cells were obtained from ATCC. Cell line authentication was performed according to the recommendations from the ATCC cell line authentication guidelines. CNE2, SUNE1, and H1299 cells were grown in RPMI 1640 medium supplemented with 10 % (vol/vol) fetal bovine serum (FBS) (Opti-Gold performance enhanced F0900-050, GenDEPOT, Barker, TX), L-glutamine, and penicillin/streptomycin, while HEK-293T cells were maintained in DMEM supplemented with 10 % (vol/vol) FBS, L-glutamine, and penicillin/streptomycin. Cells were incubated at 37 °C in a humidified atmosphere with 5 % CO2. All experiments were performed using cells within 3–10 passages. All cell lines were tested for mycoplasma

contamination using the PCR Mycoplasma Detection Kit (Applied Biological Materials Inc, USA) according to the manufacturer's instructions.

4.3. RT-qPCR

Total mRNA was extracted using TRIzol Reagent (Invitrogen) following the manufacturer's instructions. RT-qPCR was performed as described previously [25]. qPCR primers were designed using PrimerBank (https://pga.mgh.harvard.edu/primerbank/). The reaction was performed according to the following program: 50 °C for 10 min, 95 °C for 5 min, 40 cycles of 95 °C for 10 s and 60 °C for 30 s, and 95 °C for 10 min. Samples were analyzed in triplicates and normalized to GAPDH expression.

4.4. Genotyping analysis

Genomic DNA from CNE2, SUNE1, C666, and NP69 cells was isolated using the Easy-DNA kit (Invitrogen) following the manufacturer's protocol. The p53 exon was amplified using specific primers with M13 or M13R tags targeting the *TP53* exon regions [57], and then directly sequenced by GENEWIZ.

4.5. Co-IP and immunoblotting

Co-IP and immunoblotting were performed as previously described [86]. Briefly, cells were lysed in RIPA-B buffer (20 mM Na2HPO4 [pH 7.4], 150 mM NaCl, and 1 % Triton X-100) with protease inhibitors (1 mM phenylmethylsulfonyl fluoride, 5 mM NaF, 2 mM sodium orthovanadate, 3 μg/ml aprotinin, and 750 μg/ml benzamidine) by vortexing or sonication at 4 °C. For co-IP, the protein lysates were immunoprecipitated with the indicated antibodies at 4 °C overnight. The protein-antibody complexes were pulled down with 50 μl of either Protein A or G beads (Roche 11134515001 or 11243233001), washed with ice-cold RIPA-B buffer containing protease inhibitors. The washed beads were mixed with 2 × protein loading dye and boiled at 99 °C for 5 min. Lysate samples were loaded onto gels for SDS-PAGE and then transferred onto PVDF membranes (Bio-Rad Laboratories, 1620177). For immunoblotting, protein-transferred membranes were blocked with TBST buffer (10 mM Tris-HCl [pH 7.9], 150 mM NaCl, and 0.05 % Tween 20) containing 5 % skim milk, incubated with the indicated primary antibodies, subsequently incubated with HRP-conjugated secondary antibodies, and detected using ECL western blotting detection reagents (GE Healthcare, RPN2209).

4.6. p53-DNA Helix structure study

The structure of the human P53-DNA complex (PDB 1TSR) was used to examine the interface between DNA and the residues R273, R280, and D281 (chain D). Interactions between nucleotides and residues (R273 and R280) with distance <4 Å are shown by dashed lines. All molecular graphic figures were made by PyMOL.

4.7. Cycloheximide (CHX) chase assay

Protein turnover was performed as previously described [87]. Briefly, the cells were transfected with 2 μg p53(WT) and p53(R280T) plasmids, respectively for 24 h. Cells were then treated with 200 μg/mL cycloheximide and harvested at indicated time points after cycloheximide treatment. The protein levels were analyzed by immunoblotting.

4.8. Establishment of CNE2-p53KO lines

Paired guide RNA sequences targeting exon 2 and exon 4 of the *TP53* gene were designed using the optimized CRISPR design tool (http://crispr.mit.edu). DNA oligonucleotides were purchased from Integrated DNA Technologies and cloned into the pSpCas9(BB)-2A-Puro (PX459) V2.0 vector (Addgene, 62988). These *TP53* sgRNA/Cas9 constructs were transfected into CNE2 cells by electroporation. Briefly, 1×10^7 CNE2 cells were mixed with 8 μg of each *TP53* sgRNA/Cas9 plasmid in 600 μl of EmbryoMax Electroporation Buffer (Millipore, ES-003-D). Electroporation was performed at 200 V/950 μF using a Bio-Rad Gene Pulser Xcell System (Millipore). The cells were then immediately plated onto a 10 cm tissue culture plate with complete RPMI 1640 medium and selected with 3 μg/ml puromycin. Puromycin-resistant cells were seeded to form single clones in 96-well plates at a concentration of 1.5 cells per well. The p53(R280T)-knockout CNE2 (CNE2-p53KO) cells were examined by PCR to confirm the *TP53* gene deletion.

4.9. RNA-seq, GSEA, Enrichr, and metascape analyses

Cells were lysed and RNA samples were prepared by Trizol RNA isolation reagent (Thermo Fisher Scientific, 15596026). The RNA-seq was performed on BGISEQ-500 platform and mapped by BGI (Hong Kong, China). Data analysis was described previously [88,89]. The log2 ratio of FPKM (Fragments Per Kilobase of transcript per Million) between CNE2-Ctrl and CNE2-p53KO cells was calculated. A Venn diagram was generated using an online tool (http://bioinformatics.psb.ugent.be/webtools/Venn/). GSEA was employed to analyze the enrichment of p53(R280T) targets in NPC and nasopharyngeal mucosa using the public dataset (GSE118719). Enrichr-based analyses for GO_BP, BioPlanet, WikiPathways, and drug perturbations were performed using Enrichr (https://maayanlab.cloud/Enrichr/) [90]. GO and pathway analyses of p53 and p53(R280T) targets were performed using Metascape (https://metascape.org/) [91].

4.10. Generation of lentivirus and infection

2×10^6 HEK-293T cells were seeded in 10 cm tissue culture plates and maintained in complete DMEM medium overnight. The medium was replaced with 7 ml of fresh complete DMEM medium. 6 μg pCMV-dR8.2-dvpr, 2 μg pCMV-VSV-dvpr, and 8 μg lentiviral plasmids (e.g., shRNA, TetO-FUW vector [92], TetO-FUW-p53, TetO-FUW-p53 (R280T), and tTA) were mixed with 40 μL PEI in 600 μL Opti-MEM medium. The transfection mixture was incubated at room temperature for 30 min and then added to HEK-293T cells. After overnight incubation, the medium was replaced with 10 ml of complete DMEM medium. The viruses were collected 48–72 h post-transfection and concentrated using Amicon Ultra-15 centrifugal filter units (cat# UFC901024; Millipore). For viral infection, cells were seeded in 6-well plates and infected with the indicated lentiviral particles in the presence of polybrene. shRNA lentivirus-infected cells were selected using 1 μg/ml puromycin. Gene expression was examined by RT-qPCR after 84–96 h of induction.

4.11. ChIP-seq and data analysis

ChIP-seq and data analysis were performed as described previously [89]. Briefly, cells were pre-fixed for 30 min in 1.5 mM disuccinimidyl glutarate (DSG; Thermo Fisher Scientific, 20593), followed by fixation in 1 % paraformaldehyde (Thermo Fisher Scientific, 28906) at room temperature for 10 min. After glycine quenching, cell pellets were collected and lysed, then subjected to sonication using a Branson Sonifier 450 (sonication conditions: 220 cycles, power 20 %, 10s on and 10s off for CNE2-Ctrl and CNE2-p53KO cells; 80 cycles, power 18 %, 10s on and 10s off for p53-transduced CNE2-p53KO cells). The supernatant was then diluted (1:1) in the sonication buffer and subjected to immunoprecipitation with corresponding antibodies at 4 °C overnight. Beads were then washed, and DNA was reverse-crosslinked and purified. ChIP DNA was quantified, and sequencing libraries were prepared using the KAPA HyperPrep Kit (Roche, KK8502). The DNA was sequenced on an Illumina X10 platform using a PE150 kit in the UTHealth Cancer Genome Core.

The ChIP-seq data analysis was performed on the Galaxy platform

(https://usegalaxy.org/). The sequencing reads were quality-controlled by FASTQ. Cleaned reads were aligned to the human reference genome (hg19). The uniquely aligned reads were converted to bigWig format with a fragment length of 75 on the IGV browser. Peak-calling of ChIP-Seq data was performed by MACS2 with default parameters. Genomic annotations and motif analyses were performed with HOMER. ChIP-qPCR was performed using a CFX96 machine (Bio-Rad Laboratories). Forward and reverse PCR primers for amplifying the peak regions are listed in Table S2.

4.12. Cell proliferation assay and CI calculation

The cell proliferation assay was used to evaluate cell viability with thiazolyl blue tetrazolium bromide (MTT, from Sigma). 1×10^3 cells were seeded into the wells of 96-well plates. For drug treatment experiments, the following day, cells were treated with DMSO, 5-FU, and/or curcumin, then incubated for 72 h 5 mg/ml MTT reagent was added to each well, and the cells were incubated at 37 °C for 3 h. After discarding the medium, 100 μl DMSO was added to each well. The DMSO-dissolved MTT was measured using a TECAN Infinite M Plex multimode microplate reader with spectrophotometric absorbance (OD570). The inhibition ratios of cell survival were calculated as: 100 % × Nt/Nc, where Nt is the optical density of the treatment group and Nc is the optical density of the control group. CI calculation was performed using CompuSyn software and used to quantitatively determine the combination effect of curcumin and 5-FU (CI < 1 means synergistic effect; CI = 1 means additive effect; CI > 1 means antagonistic effect).

4.13. Colony forming assay

Colony-formation assay was performed as described previously [93]. Briefly, CNE2 and SUNE1 cells were plated in 6-well culture plates at various densities (5×10^2–1×10^3 cells per well) for 12 h, then exposed to 5-FU and/or curcumin for 3 days. The cells were then maintained for an additional 5–7 days with fresh RPMI 1640 medium. Surviving colonies (defined as ≥ 50 cells) were counted. Plating efficiencies (PE) were calculated as the number of colonies divided by the number of cells seeded. The survival fraction was calculated as the PE of the drug-treated group divided by the controls (e.g., control shRNA or DMSO). Three independent experiments were performed.

4.14. Flow Cytometric analysis

G0/G1, G2, S, and subG1 phase cells were analyzed by flow cytometry as described previously [94]. Briefly, cells were plated in 6-well plates (2.5×10^5 per well) for 12 h, then treated with DMSO and 5-FU (30 μM) for 48 h. Cells were harvested, washed with 1 ml PBS, and fixed in 70 % ethanol for 30 min at 4 °C. They were then washed twice with PBS, resuspended in 500 μl flow cytometry buffer (1 % FBS and 1 % penicillin/streptomycin in Ca2+ and Mg2+ free PBS) with ribonuclease (1 μg/ml). The cell solutions were incubated with 5 μl PI on ice in the dark for 30 min. Cells were immediately examined on a BD LSR II flow cytometer (BD Biosciences) and analyzed using FlowJo v10.

4.15. γH2AX Immunofluorescent staining

Cells were grown to 70 % confluence in 12-well plates, then fixed with 4 % paraformaldehyde (Affymetrix) for 10 min. After fixation, cells were washed twice with 500 μl wash buffer (PBS with 1 % BSA; Fisher Scientific), followed by blocking in PBS containing 10 % donkey serum (Jackson ImmunoResearch Labs), 1 % BSA, and 0.3 % Triton X-100 (Sigma) for 1 h. Cells were then incubated with the primary antibody (anti-phospho-Histone H2A.X (Ser139), Sigma, clone JBW301), diluted 1:1000 in antibody dilution buffer (PBS with 1 % BSA, 1 % donkey serum, and 0.3 % Triton X-100), at 4 °C overnight with gentle rocking. Following incubation, cells were washed twice. Where appropriate, a secondary antibody (goat anti-mouse IgG (H + L)-HRP, Invitrogen, Cat# 31430, 1:5000 diluted in dilution buffer) was added and incubated for 1 h at room temperature, protected from light. This was followed by two additional washes, and counterstaining with DAPI diluted in dilution buffer. Finally, cells were washed twice and stored in PBS for visualization. Images were taken under a Leica DMi8 microscope.

4.16. CAM assay

In ovo CAM assay was described previously [57]. Briefly, 1.5×10^6 (for assays in Fig. 2E) – 4×10^6 cells (for assays in Fig. 6I) (PBS mixed with Matrigel: 1:1) were implanted onto the CAM of 8-day-old chick embryos (Texas A&M University). For drug treatment experiments, 1×10^6 CNE2, CNE2-shCtrl, CNE2-shp53-1, and CNE2-shp53-2 cells were plated in 100 mm culture plates for 12 h, then exposed to 8 μM 5-FU, 4 μM curcumin, or a combination for 3 days (DMSO as control). Then cells were detached and counted using a hemocytometer, then resuspended in PBS/Matrigel (1:1) and implanted onto the CAM. A silicon ring was employed to restrict the motion of cells within the injection area. On day 5, CAMs/tumors were photographed and resected, minced, dissociated into a single-cell suspension with type II collagenase (Roche), plated on dishes, and counted using a hemocytometer.

4.17. Xenograft NPC model

The animal studies were approved by the Animal Ethics and Welfare Committee of Sun Yat-sen University (SYSU-IACUC-2023-000658). Male BALB/c nude mice (5–6 weeks old, 16–20 g) were purchased from GemPharmatech (Nanjing, Jiangsu, China). To explore the role of p53 (R280T) in NPC cells, CNE2 and CNE2-p53KO cells (2×10^6 cells/mouse) were injected subcutaneously into the right hind flank of the nude mice. Tumor length and width were measured every 3 days, and the mice were sacrificed after 40 days. Tumor volume was calculated using the formula (length × width^2)/2. To verify the synergistic effect of 5-FU and curcumin in NPC cells, CNE2 cell xenograft mice (2×10^6 cells/mouse) were divided into four groups: the control group, 5-FU group, curcumin group, and combination group. After several days, when tumor size reached 100 mm^3, mice were administered curcumin (50 mg/kg, corn oil) or 5-FU (25 mg/kg, PBS) by intraperitoneal (IP) injection 3 times per week, totaling 8 injections after tumor inoculation. The control group was treated with PBS and corn oil. Tumor length and width were measured every 3 days, and the mice were sacrificed after 33 days. Tumor volume was calculated using the formula (length × width^2)/2.

4.18. Apoptotic activity assay

Caspase 3/7 activity was described previously [94]. Apoptosis was measured via Caspase 3/7 activity using the SensoLyte Homogeneous AMC Caspase-3/7 Assay Kit (Anaspec, AS-71118). The assay was carried out according to the manufacturer's instructions. CNE2-shCtrl and CNE2-shKMT5B cells were cultured in a 6-well plate and then treated with 10 μM 5-FU for 2 days. Cell lysates were incubated with Caspase 3/7 fluorogenic substrate for 6 h. Fluorescence was measured at Ex/Em = 354 nm/442 nm using the TECAN Infinite M Plex multimode microplate reader.

4.19. Drug screening

Drug screening was conducted in CNE2 cells to identify compounds that downregulate *KMT5B* mRNA expression. 1×10^3 CNE2 cells were seeded into 96-well plates and treated with the indicated compounds the following day. After 24 h of incubation, the total mRNA was extracted using TRIzol Reagent (Invitrogen) according to the manufacturer's instructions. RT-qPCR was performed as previously described. Compound concentrations were selected based on their respective IC_{50} values,

which are listed in the table below.

Compound	Concentration	Solvent
Pramlintide	30 μg/mL	ddH2O
Theophylline	50 μM	DMSO
Itraconazole	0.1 μM	DMSO
Miconazole	50 μM	DMSO
Rifabutin	5 μM	DMSO
Perampanel	180 μM	DMSO
2-Deoxy-D-glucose (2DG)	4 mM	ddH2O
JIB-04	10 nM	DMSO
CX-5461	150 nM	DMSO
BMH-21	3 μM	DMSO
Actinomycin D (ActD)	10 ng/mL	DMSO
SB202190	20 μM	DMSO
AZD2811	1 μM	DMSO
AZD7762	1 μM	DMSO
Mecamylamine	400 μM	DMSO
Zatebradine	2 μM	DMSO
AZD8330	1 μM	DMSO
BI 2536	10 nM	DMSO
OICR-9429	5 μM	DMSO
EC359	10 nM	DMSO
BAY-1816032	6.1 nM	DMSO
IACS-010759	1 μM	DMSO
Rotenone	13 μM	DMSO
IWPA	5 μM	DMSO
Etoposide	10 μM	DMSO
Curcumin	4 μM	DMSO

CRediT authorship contribution statement

Haidan Luo: Writing – original draft, Methodology, Investigation, Formal analysis, Data curation. **Mo-Fan Huang:** Investigation, Formal analysis, Data curation. **An Xu:** Methodology, Formal analysis, Data curation. **Donghui Wang:** Investigation, Data curation. **Julian A. Gingold:** Writing – review & editing, Software, Resources, Methodology. **Jian Tu:** Methodology, Formal analysis, Data curation. **Ruoyu Wang:** Software, Methodology, Formal analysis. **Zijun Huo:** Methodology, Investigation. **Yen-Ting Chiang:** Software, Methodology, Formal analysis. **Kuang-Lei Tsai:** Methodology, Formal analysis, Data curation. **Jie Su:** Formal analysis, Data curation. **Danielle A. Bazer:** Writing – review & editing, Methodology, Formal analysis. **Mien-Chie Hung:** Writing – review & editing, Supervision, Resources, Funding acquisition. **Canmao Xie:** Project administration, Funding acquisition. **Yubiao Guo:** Supervision, Funding acquisition, Conceptualization. **Dung-Fang Lee:** Writing – review & editing, Supervision, Resources, Project administration, Funding acquisition, Conceptualization. **Huiling Yang:** Supervision, Resources, Funding acquisition, Conceptualization. **Ruiying Zhao:** Writing – review & editing, Supervision, Resources, Funding acquisition, Conceptualization.

Data availability

The data supporting the findings of this study are available within the paper and its Supplemental Information. The RNA-seq and ChIP-seq data are available in the Gene Expression Omnibus (GEO) repository under accession numbers GSE198338.

5.1. Statistical analysis

All data are presented as mean ± standard deviation (SD). The statistical significance of mean values among different groups was determined using two-way ANOVA followed by Student's t-test. All statistical analyses were performed using SPSS 19.0 and GraphPad Prism 7. Data were considered statistically significant when *$p \leq 0.05$, **$p < 0.01$, ***$p < 0.001$, and ****$p < 0.0001$.

Declaration of competing interest

The authors declare that they have no known competing financial interests or personal relationships that could have appeared to influence the work reported in this paper.

Acknowledgements

The authors gratefully acknowledge Ying Liu and Trinh TT Phan for their contributions to laboratory management, reagent preparation, and valuable suggestions during the revision process. We also thank Yi-Hung Chen and Mei-Kuang Chen for their experimental support. A.X. was supported by the CPRIT UTHealth BIG-TCR training program. R.Z. was supported by UTHealth/IBP P37516-11999 and NIH/NCI R01CA246130. D.-F.L. was supported by CPRIT RR160019, NIH/NCI R01CA246130, DoD RCRP HT9425-24-1-0957, the Rolanette and Berdon Lawrence Bone Disease Program of Texas, and the Pablove Foundation Childhood Cancer Research Grant (690785). Dung-Fang Lee is a CPRIT Scholar in Cancer Research. H.Y. was supported by grants from the National Natural Science Foundation of China (81874127) and the Scientific and Technological Project of Guangdong, China (2015A020211006). C.X. was supported by grants from the Guangdong Finance Foundation for Industrial Technology Research and Development, China (20160907).

Appendix A. Supplementary data

Supplementary data to this article can be found online at https://doi.org/10.1016/j.canlet.2025.217736.

Table S1
shRNA information

shRNA	Target sequence
shCtrl	CTTACGCTGAGTACTTCGA
shp53-1	GACTCCAGTGGTAATCTACT
shp53-2	GTGCCTGTCCTGGGAGAGA
shKMT5B-1	GTGAGATTTAGGCCTATTAAA
shKMT5B-2	CATCTAAGCTAACTCATATAA

Table S2
RT-qPCR primers used for this study

Gene	5′ Primer sequence	3′ Primer sequence	PCR size (bp)
CDKN1A	TGTCCGTCAGAACCCATGC	AAAGTCGAAGTTCCATCGCTC	139
PUMA (BBC3)	GCCAGATTTGTGAGACAAGAGG	CAGGCACCTAATTGGGCTC	136
BAX	CCCGAGAGGTCTTTTTCCGAG	CCAGCCCATGATGGTTCTGAT	155
MDM2	GAATCATCGGACTCAGGTACATC	TCTGTCTCACTAATTGCTCTCCT	167
14-3-3σ (SFN)	TGACGACAAGAAGCGCATCAT	GTAGTGGAAGACGGAAAAGTTCA	133
p53	CAGCACATGACGGAGGTTGT	CCAGACCATCGCTATCTGAGC	125
CCNG2	TCTCGGGTTGTTGAACGTCTA	GTAGCCTCAATCAAACTCAGCC	81
KMT5B	AGGACAGAGTCGCTATGTACC	CAAACTGGTTGCTAGGTCATCAT	79
GAPDH	CCACTCCTCCACCTTTGAC	ACCCTGTTGCTGTAGCCA	102

The qPCR reaction was performed using the following program: 50 °C for 10 min, 95 °C for 5 min, followed by 40 cycles of 95 °C for 10 s and 60 °C for 30 s, with a final step at 95 °C for 10 min.

References

[1] F. Bray, M. Laversanne, H. Sung, J. Ferlay, R.L. Siegel, I. Soerjomataram, A. Jemal, Global cancer statistics 2022: GLOBOCAN estimates of incidence and mortality worldwide for 36 cancers in 185 countries, CA Cancer J. Clin. 74 (2024) 229–263.

[2] S. Cao, The Epidemiology of Nasopharyngeal Carcinoma, 2023.

[3] W.M. Yu, S.S. Hussain, Incidence of nasopharyngeal carcinoma in Chinese immigrants, compared with Chinese in China and South East Asia: review, J. Laryngol. Otol. 123 (2009) 1067–1074, https://doi.org/10.1017/S0022215109005623.

[4] H.Y. Wang, Y.L. Chang, K.F. To, J.S. Hwang, H.Q. Mai, Y.F. Feng, E.T. Chang, C. P. Wang, M.K. Kam, S.L. Cheah, M. Lee, L. Gao, H.Z. Zhang, J.H. He, H. Jiang, P. Q. Ma, X.D. Zhu, L. Zeng, C.Y. Chen, G. Chen, M.Y. Huang, S. Fu, Q. Shao, A.J. Han, H.G. Li, C.K. Shao, P.Y. Huang, C.N. Qian, T.X. Lu, J.T. Li, W. Ye, I. Ernberg, H. K. Ng, J.T. Wee, Y.X. Zeng, H.O. Adami, A.T. Chan, J.Y. Shao, A new prognostic histopathologic classification of nasopharyngeal carcinoma, Chin. J. Cancer 35 (2016) 41.

[5] K.C.W. Wong, E.P. Hui, K.W. Lo, W.K.J. Lam, D. Johnson, L. Li, Q. Tao, K.C. A. Chan, K.F. To, A.D. King, B.B.Y. Ma, A.T.C. Chan, Nasopharyngeal carcinoma: an evolving paradigm, Nat. Rev. Clin. Oncol. 18 (2021) 679–695.

[6] R. Pathmanathan, U. Prasad, G. Chandrika, R. Sadler, K. Flynn, N. Raab-Traub, Undifferentiated, nonkeratinizing, and squamous cell carcinoma of the nasopharynx. Variants of Epstein-Barr virus-infected neoplasia, Am. J. Pathol. 146 (1995) 1355–1367.

[7] L.S. Young, C.W. Dawson, Epstein-Barr virus and nasopharyngeal carcinoma, Chin. J. Cancer 33 (2014) 581–590.

[8] D.C. Lin, X. Meng, M. Hazawa, Y. Nagata, A.M. Varela, L. Xu, Y. Sato, L.Z. Liu, L. W. Ding, A. Sharma, B.C. Goh, S.C. Lee, B.F. Petersson, F.G. Yu, P. Macary, M.Z. Oo, C.S. Ha, H. Yang, S. Ogawa, K.S. Loh, H.P. Koeffler, The genomic landscape of nasopharyngeal carcinoma, Nat. Genet. 46 (2014) 866–871.

[9] L. Zhang, K.D. MacIsaac, T. Zhou, P.Y. Huang, C. Xin, J.R. Dobson, K. Yu, D. Y. Chiang, Y. Fan, M. Pelletier, Y. Wang, S. Jaeger, V. Krishnamurthy Radhakrishnan, L. JeBailey, P. Skewes-Cox, J. Zhang, W. Fang, Y. Huang, H. Zhao, Y. Zhao, E. Li, B. Peng, A. Huang, G. Dranoff, P.S. Hammerman, J. Engelman, H. Bitter, Y.X. Zeng, Y. Yao, Genomic analysis of nasopharyngeal carcinoma reveals TME-based subtypes, Mol. Cancer Res. 15 (2017) 1722–1732.

[10] J. Li, M. Guo, L. Chen, Z. Chen, Y. Fu, Y. Chen, Amyloid aggregates induced by the p53-R280T mutation lead to loss of p53 function in nasopharyngeal carcinoma, Cell Death Dis. 15 (2024) 35.

[11] K.H. Vousden, C. Prives, Blinded by the light: the growing complexity of p53, Cell 137 (2009) 413–431.

[12] E.R. Kastenhuber, S.W. Lowe, Putting p53 in context, Cell 170 (2017) 1062–1078.

[13] R. Zhou, A. Xu, J. Gingold, L.C. Strong, R. Zhao, D.F. Lee, Li-fraumeni syndrome disease model: a platform to develop precision cancer therapy targeting oncogenic p53, Trends Pharmacol. Sci. 38 (2017) 908–927.

[14] A.B. Williams, B. Schumacher, p53 in the DNA-Damage-Repair Process, Cold Spring Harb. Perspect. Med. 6 (2016).

[15] J. Bargonetti, C. Prives, Gain-of-function mutant p53: history and speculation, J. Mol. Cell Biol. 11 (2019) 605–609.

[16] C. Kandoth, M.D. McLellan, F. Vandin, K. Ye, B. Niu, C. Lu, M. Xie, Q. Zhang, J. F. McMichael, M.A. Wyczalkowski, M.D.M. Leiserson, C.A. Miller, J.S. Welch, M. J. Walter, M.C. Wendl, T.J. Ley, R.K. Wilson, B.J. Raphael, L. Ding, Mutational landscape and significance across 12 major cancer types, Nature 502 (2013) 333–339.

[17] T. Soussi, K.G. Wiman, TP53: an oncogene in disguise, Cell Death Differ. 22 (2015) 1239–1249.

[18] W. Zhang, W. Qian, J. Gu, M. Gong, W. Zhang, S. Zhang, C. Zhou, Z. Jiang, J. Jiang, L. Han, X. Wang, Z. Wu, Q. Ma, Z. Wang, Mutant p53 driven-LINC00857, a protein scaffold between FOXM1 and deubiquitinase OTUB1, promotes the metastasis of pancreatic cancer, Cancer Lett. 552 (2023) 215976.

[19] R. Feng, Y. Yin, Y. Wei, Y. Li, L. Li, R. Zhu, X. Yu, Y. Liu, Y. Zhao, Z. Liu, Mutant p53 activates hnRNPA2B1-AGAP1-mediated exosome formation to promote esophageal squamous cell carcinoma progression, Cancer Lett. 562 (2023) 216154.

[20] S. Ling, Q. Shan, Q. Zhan, Q. Ye, P. Liu, S. Xu, X. He, J. Ma, J. Xiang, G. Jiang, X. Wen, Z. Feng, Y. Wu, T. Feng, L. Xu, K. Chen, X. Zhang, R. Wei, C. Zhang, B. Cen, H. Xie, P. Song, J. Liu, S. Zheng, X. Xu, USP22 promotes hypoxia-induced hepatocellular carcinoma stemness by a HIF1α/USP22 positive feedback loop upon TP53 inactivation, Gut 69 (2020) 1322–1334.

[21] Y. Yang, H. Yuan, L. Zhao, S. Guo, S. Hu, M. Tian, Y. Nie, J. Yu, C. Zhou, J. Niu, G. Wang, Y. Song, Targeting the miR-34a/LRPPRC/MDR1 axis collapse the chemoresistance in P53 inactive colorectal cancer, Cell Death Differ. 29 (2022) 2177–2189.

[22] X. Cao, J. Hou, Q. An, Y.G. Assaraf, X. Wang, Towards the overcoming of anticancer drug resistance mediated by p53 mutations, Drug Resist. Updates 49 (2020) 100671.

[23] J. Zhu, M.A. Sammons, G. Donahue, Z. Dou, M. Vedadi, M. Getlik, D. Barsyte-Lovejoy, R. Al-awar, B.W. Katona, A. Shilatifard, J. Huang, X. Hua, C. H. Arrowsmith, S.L. Berger, Gain-of-function p53 mutants co-opt chromatin pathways to drive cancer growth, Nature 525 (2015) 206–211.

[24] R. Shoemaker, M.F. Huang, Y.S. Wu, C.S. Huang, D.F. Lee, Decoding the molecular symphony: interactions between the m(6)A and p53 signaling pathways in cancer, NAR Cancer 6 (2024) zcae037.

[25] A. Xu, M. Liu, M.F. Huang, Y. Zhang, R. Hu, J.A. Gingold, Y. Liu, D. Zhu, C. S. Chien, W.C. Wang, Z. Liao, F. Yuan, C.W. Hsu, J. Tu, Y. Yu, T. Rosen, F. Xiong, P. Jia, Y.P. Yang, D.A. Bazer, Y.W. Chen, W. Li, C.D. Huff, J.J. Zhu, F. Aguilo, S. H. Chiou, N.C. Boles, C.C. Lai, M.C. Hung, Z. Zhao, E.L. Van Nostrand, R. Zhao, D. F. Lee, Rewired m(6)A epitranscriptomic networks link mutant p53 to neoplastic transformation, Nat. Commun. 14 (2023) 1694.

[26] V.J.N. Bykov, S.E. Eriksson, J. Bianchi, K.G. Wiman, Targeting mutant p53 for efficient cancer therapy, Nat. Rev. Cancer 18 (2018) 89–102.

[27] X. Zhou, Q. Hao, H. Lu, Mutant p53 in cancer therapy-the barrier or the path, J. Mol. Cell Biol. 11 (2019) 293–305.

[28] M.D. Wilkie, E.A. Anaam, A.S. Lau, C.P. Rubbi, T.M. Jones, M.T. Boyd, N. Vlatković, TP53 mutations in head and neck cancer cells determine the Warburg phenotypic switch creating metabolic vulnerabilities and therapeutic opportunities for stratified therapies, Cancer Lett. 478 (2020) 107–121.

[29] F. Niehr, T. Eder, T. Pilz, R. Konschak, D. Treue, F. Klauschen, M. Bockmayr, S. Türkmen, K. Jöhrens, V. Budach, I. Tinhofer, Multilayered omics-based analysis of a head and neck cancer model of cisplatin resistance reveals intratumoral heterogeneity and treatment-induced clonal selection, Clin. Cancer Res. 24 (2018) 158–168.

[30] D.H. Geschwind, M.W. State, Gene hunting in autism spectrum disorder: on the path to precision medicine, Lancet Neurol. 14 (2015) 1109–1120.

[31] G. Chen, L. Han, S. Tan, X. Jia, H. Wu, Y. Quan, Q. Zhang, B. Yu, Z. Hu, K. Xia, H. Guo, Loss-of-function of KMT5B leads to neurodevelopmental disorder and impairs neuronal development and neurogenesis, Journal of genetics and genomics = Yi chuan xue bao 49 (2022) 881–890.

[32] K.L. Paquin, N.G. Howlett, Understanding the histone DNA repair code: H4K20me2 makes its mark, Mol. Cancer Res. : MCR 16 (2018) 1335–1345.

[33] Z.J. Wang, B. Rein, P. Zhong, J. Williams, Q. Cao, F. Yang, F. Zhang, K. Ma, Z. Yan, Autism risk gene KMT5B deficiency in prefrontal cortex induces synaptic dysfunction and social deficits via alterations of DNA repair and gene transcription, Neuropsychopharmacology 46 (2021) 1617–1626.

[34] H. Kato, S. Hayami, M. Ueno, N. Suzaki, M. Nakamura, T. Yoshimura, A. Miyamoto, Y. Shigekawa, K.I. Okada, M. Miyazawa, Y. Kitahata, S. Ehata, R. Hamamoto, H. Yamaue, M. Kawai, Histone methyltransferase SUV420H1/KMT5B contributes to poor prognosis in hepatocellular carcinoma, Cancer Sci. 115 (2024) 385–400.

[35] J.J. Caudell, M.L. Gillison, E. Maghami, S. Spencer, D.G. Pfister, D. Adkins, A. C. Birkeland, D.M. Brizel, P.M. Busse, A.J. Cmelak, A.D. Colevas, D.W. Eisele, T. Galloway, J.L. Geiger, R.I. Haddad, W.L. Hicks, Y.J. Hitchcock, A. Jimeno, D. Leizman, L.K. Mell, B.B. Mittal, H.A. Pinto, J.W. Rocco, C.P. Rodriguez, P. S. Savvides, D. Schwartz, J.P. Shah, D. Sher, M. St John, R.S. Weber, G. Weinstein, F. Worden, J. Yang Bruce, S.S. Yom, W. Zhen, J.L. Burns, S.D. Darlow, NCCN Guidelines® insights: head and neck cancers, version 1.2022, J Natl Compr Canc Netw 20 (2022) 224–234.

[36] P. Blanchard, A. Lee, S. Marguet, J. Leclercq, W.T. Ng, J. Ma, A.T. Chan, P. Y. Huang, E. Benhamou, G. Zhu, D.T. Chua, Y. Chen, H.Q. Mai, D.L. Kwong, S. L. Cheah, J. Moon, Y. Tung, K.H. Chi, G. Fountzilas, L. Zhang, E.P. Hui, T.X. Lu, J. Bourhis, J.P. Pignon, M.-N.C. Group, Chemotherapy and radiotherapy in nasopharyngeal carcinoma: an update of the MAC-NPC meta-analysis, Lancet Oncol. 16 (2015) 645–655.

[37] D.G. Pfister, S. Spencer, D. Adelstein, D. Adkins, Y. Anzai, D.M. Brizel, J.Y. Bruce, P.M. Busse, J.J. Caudell, A.J. Cmelak, A.D. Colevas, D.W. Eisele, M. Fenton, R. L. Foote, T. Galloway, M.L. Gillison, R.I. Haddad, W.L. Hicks, Y.J. Hitchcock, A. Jimeno, D. Leizman, E. Maghami, L.K. Mell, B.B. Mittal, H.A. Pinto, J.A. Ridge, J.W. Rocco, C.P. Rodriguez, J.P. Shah, R.S. Weber, G. Weinstein, M. Witek, F. Worden, S.S. Yom, W. Zhen, J.L. Burns, S.D. Darlow, Head and neck cancers, version 2.2020, NCCN clinical practice guidelines in oncology, J. Natl. Compr. Cancer Netw. : J. Natl. Compr. Cancer Netw. 18 (2020) 873–898.

[38] Y.P. Chen, N. Ismaila, M.L.K. Chua, A.D. Colevas, R. Haddad, S.H. Huang, J.T. S. Wee, A.C. Whitley, J.L. Yi, S.S. Yom, A.T.C. Chan, C.S. Hu, J.Y. Lang, Q.T. Le, A. W.M. Lee, N. Lee, J.C. Lin, B. Ma, T.J. Morgan, J. Shah, Y. Sun, J. Ma, Chemotherapy in combination with radiotherapy for definitive-intent treatment of stage II-IVA nasopharyngeal carcinoma: CSCO and ASCO guideline, J. Clin. Oncol. : official journal of the American Society of Clinical Oncology 39 (2021) 840–859.

[39] P.M. De Angelis, D.H. Svendsrud, K.L. Kravik, T. Stokke, Cellular response to 5-fluorouracil (5-FU) in 5-FU-resistant colon cancer cell lines during treatment and recovery, Mol. Cancer 5 (2006) 20.

[40] Y. Lei, Y.Q. Li, W. Jiang, X.H. Hong, W.X. Ge, Y. Zhang, W.H. Hu, Y.Q. Wang, Y. L. Liang, J.Y. Li, W.C.S. Cho, J.P. Yun, J. Zeng, J.W. Chen, L.Z. Liu, L. Li, L. Chen, F. Y. Xie, W.F. Li, Y.P. Mao, X. Liu, Y.P. Chen, L.L. Tang, Y. Sun, N. Liu, J. Ma, A gene-expression predictor for efficacy of induction chemotherapy in locoregionally advanced nasopharyngeal carcinoma, J. Natl. Cancer Inst. 113 (2021) 471–480.

[41] H. Peng, L. Chen, W.F. Li, R. Guo, Y.P. Mao, Y. Zhang, Y. Guo, Y. Sun, J. Ma, Tumor response to neoadjuvant chemotherapy predicts long-term survival outcomes in patients with locoregionally advanced nasopharyngeal carcinoma: a secondary analysis of a randomized phase 3 clinical trial, Cancer 123 (2017) 1643–1652.

[42] Q. Zeng, Z. Wang, C. Liu, Z. Gong, L. Yang, L. Jiang, Z. Ma, Y. Qian, Y. Yang, H. Kang, S. Hong, Y. Bu, G. Hu, Knockdown of NFBD1/MDC1 enhances chemosensitivity to cisplatin or 5-fluorouracil in nasopharyngeal carcinoma CNE1 cells, Mol. Cell. Biochem. 418 (2016) 137–146.

[43] L. Qin, X. Zhang, L. Zhang, Y. Feng, G.X. Weng, M.Z. Li, Q.L. Kong, C.N. Qian, Y. X. Zeng, M.S. Zeng, D.F. Liao, L.B. Song, Downregulation of BMI-1 enhances 5-fluorouracil-induced apoptosis in nasopharyngeal carcinoma cells, Biochem. Biophys. Res. Commun. 371 (2008) 531–535.

[44] J. Lin, H. Qin, Y. Han, X. Li, Y. Zhao, G. Zhai, CircNRIP1 modulates the miR-515-5p/IL-25 Axis to control 5-Fu and cisplatin resistance in nasopharyngeal carcinoma, Drug Des. Dev. Ther. 15 (2021) 323–330.

[45] W. Yim-im, O. Sawatdichaikul, S. Semsri, N. Horata, W. Mokmak, S. Tongsima, A. Suksamrarn, K. Choowongkomon, Computational analyses of curcuminoid analogs against kinase domain of HER2, BMC Bioinf. 15 (2014) 261.

[46] A. Catania, E. Barrajon-Catalan, S. Nicolosi, F. Cicirata, V. Micol, Immunoliposome encapsulation increases cytotoxic activity and selectivity of curcumin and resveratrol against HER2 overexpressing human breast cancer cells, Breast Cancer Res. Treat. 141 (2013) 55–65.

[47] X.D. Sun, X.E. Liu, D.S. Huang, Curcumin induces apoptosis of triple-negative breast cancer cells by inhibition of EGFR expression, Mol. Med. Rep. 6 (2012) 1267–1270.

[48] B. Chen, Y. Zhang, Y. Wang, J. Rao, X. Jiang, Z. Xu, Curcumin inhibits proliferation of breast cancer cells through Nrf2-mediated down-regulation of Fen1 expression, J. Steroid Biochem. Mol. Biol. 143 (2014) 11–18.

[49] L. Wu, L. Guo, Y. Liang, X. Liu, L. Jiang, L. Wang, Curcumin suppresses stem-like traits of lung cancer cells via inhibiting the JAK2/STAT3 signaling pathway, Oncol. Rep. 34 (2015) 3311–3317.

[50] X. Xue, J.L. Yu, D.Q. Sun, F. Kong, X.J. Qu, W. Zou, J. Wu, R.M. Wang, Curcumin induces apoptosis in SGC-7901 gastric adenocarcinoma cells via regulation of mitochondrial signaling pathways, Asian Pac J Cancer Prev 15 (2014) 3987–3992.

[51] J. Yang, D. Zhu, S. Liu, M. Shao, Y. Liu, A. Li, Y. Lv, M. Huang, D. Lou, Q. Fan, Curcumin enhances radiosensitization of nasopharyngeal carcinoma by regulating circRNA network, Mol. Carcinog. 59 (2020) 202–214.

[52] A.A. Momtazi-Borojeni, F. Ghasemi, A. Hesari, M. Majeed, M. Caraglia, A. Sahebkar, Anti-cancer and radio-sensitizing effects of curcumin in nasopharyngeal carcinoma, Curr. Pharm. Des. 24 (2018) 2121–2128.

[53] D. Zhu, M. Shao, J. Yang, M. Fang, S. Liu, D. Lou, R. Gao, Y. Liu, A. Li, Y. Lv, Z. Mo, Q. Fan, Curcumin enhances radiosensitization of nasopharyngeal carcinoma via mediating regulation of tumor stem-like cells by a CircRNA network, J. Cancer 11 (2020) 2360–2370.

[54] C. Liu, M. Rokavec, Z. Huang, H. Hermeking, Curcumin activates a ROS/KEAP1/NRF2/miR-34a/b/c cascade to suppress colorectal cancer metastasis, Cell Death Differ. 30 (2023) 1771–1785.

[55] C. Karavasili, D.A. Andreadis, O.L. Katsamenis, E. Panteris, P. Anastasiadou, Z. Kakazanis, V. Zoumpourlis, C.K. Markopoulou, S. Koutsopoulos, I. S. Vizirianakis, D.G. Fatouros, Synergistic antitumor potency of a self-assembling peptide hydrogel for the local Co-delivery of doxorubicin and curcumin in the treatment of head and neck cancer, Mol. Pharm. 16 (2019) 2326–2341.

[56] G. Guney Eskiler, E. Sahin, A. Deveci Ozkan, O.T. Cilingir Kaya, S. Kaleli, Curcumin induces DNA damage by mediating homologous recombination mechanism in triple negative breast cancer, Nutr. Cancer 72 (2020) 1057–1066.

[57] D.F. Lee, J. Su, H.S. Kim, B. Chang, D. Papatsenko, R. Zhao, Y. Yuan, J. Gingold, W. Xia, H. Darr, R. Mirzayans, M.C. Hung, C. Schaniel, I.R. Lemischka, Modeling familial cancer with induced pluripotent stem cells, Cell 161 (2015) 240–254.

[58] H. Kim, S. Yoo, R. Zhou, A. Xu, J.M. Bernitz, Y. Yuan, A.M. Gomes, M.G. Daniel, J. Su, E.G. Demicco, J. Zhu, K.A. Moore, D.F. Lee, I.R. Lemischka, C. Schaniel, Oncogenic role of SFRP2 in p53-mutant osteosarcoma development via autocrine and paracrine mechanism, Proc. Natl. Acad. Sci. U. S. A. 115 (2018) E11128–E11137.

[59] J.H. Choe, T. Kawase, A. Xu, A. Guzman, A.Z. Obradovic, A.M. Low-Calle, B. Alaghebandan, A. Raghavan, K. Long, P.M. Hwang, J.D. Schiffman, Y. Zhu, R. Zhao, D.F. Lee, C. Katz, C. Prives, Li-fraumeni syndrome-associated dimer-forming mutant p53 promotes transactivation-independent mitochondrial cell death, Cancer Discov. 13 (2023) 1250–1273.

[60] D. Chachad, L.R. Patel, C.V. Recio, R. Pourebrahim, E.M. Whitley, W. Wang, X. Su, A. Xu, D.F. Lee, G. Lozano, Unique transcriptional profiles underlie osteosarcomagenesis driven by different p53 mutants, Cancer Res. 83 (2023) 2297–2311.

[61] J. Gencel-Augusto, X. Su, Y. Qi, E.M. Whitley, V. Pant, S. Xiong, V. Shah, J. Lin, E. Perez, M.L. Fiorotto, I. Mahmud, A.K. Jain, P.L. Lorenzi, N.E. Navin, E.R. Richie, G. Lozano, Dimeric p53 mutant elicits unique tumor-suppressive activities through an altered metabolic program, Cancer Discov. 13 (2023) 1230–1249.

[62] S. Garritano, A. Inga, F. Gemignani, S. Landi, More targets, more pathways and more clues for mutant p53, Oncogenesis 2 (2013) e54.

[63] M.D. Wyatt, D.M. Wilson 3rd, Participation of DNA repair in the response to 5-fluorouracil, Cell. Mol. Life Sci. 66 (2009) 788–799.

[64] M. Zimmermann, A.S. Arachchige-Don, M.S. Donaldson, R.F. Dallapiazza, C. E. Cowan, M.C. Horne, Elevated cyclin G2 expression intersects with DNA damage checkpoint signaling and is required for a potent G2/M checkpoint arrest response to doxorubicin, J. Biol. Chem. 287 (2012) 22838–22853.

[65] C.T. Tuzon, T. Spektor, X. Kong, L.M. Congdon, S. Wu, G. Schotta, K. Yokomori, J. C. Rice, Concerted activities of distinct H4K20 methyltransferases at DNA double-strand breaks regulate 53BP1 nucleation and NHEJ-directed repair, Cell Rep. 8 (2014) 430–438.

[66] M.V. Botuyan, J. Lee, I.M. Ward, J.E. Kim, J.R. Thompson, J. Chen, G. Mer, Structural basis for the methylation state-specific recognition of histone H4-K20 by 53BP1 and Crb2 in DNA repair, Cell 127 (2006) 1361–1373.

[67] K. Matsuzaki, S. Kondo, T. Ishikawa, A. Shinohara, Human RAD51 paralogue SWSAP1 fosters RAD51 filament by regulating the anti-recombinase FIGNL1 AAA+ ATPase, Nat. Commun. 10 (2019) 1407.

[68] J. Martino, G.J. Brunette, J. Barroso-Gonzalez, T.N. Moiseeva, C.M. Smith, C. J. Bakkenist, R.J. O'Sullivan, K.A. Bernstein, The human Shu complex functions with PDS5B and SPIDR to promote homologous recombination, Nucleic Acids Res. 47 (2019) 10151–10165.

[69] W. Wei, Z. Ba, M. Gao, Y. Wu, Y. Ma, S. Amiard, C.I. White, J.M. Rendtlew Danielsen, Y.G. Yang, Y. Qi, A role for small RNAs in DNA double-strand break repair, Cell 149 (2012) 101–112.

[70] T.C. Chou, Drug combination studies and their synergy quantification using the Chou-Talalay method, Cancer Res. 70 (2010) 440–446.

[71] T.C. Chou, P. Talalay, Quantitative analysis of dose-effect relationships: the combined effects of multiple drugs or enzyme inhibitors, Adv. Enzym. Regul. 22 (1984) 27–55.

[72] T. Soussi, K.G. Wiman, Shaping genetic alterations in human cancer: the p53 mutation paradigm, Cancer Cell 12 (2007) 303–312.

[73] P.M. Do, L. Varanasi, S. Fan, C. Li, I. Kubacka, V. Newman, K. Chauhan, S. R. Daniels, M. Boccetta, M.R. Garrett, R. Li, L.A. Martinez, Mutant p53 cooperates with ETS2 to promote etoposide resistance, Genes Dev. 26 (2012) 830–845.

[74] Y. Jia, Y. Chen, M. Chen, M. He, S. Xu, H. Li, X. Lin, L. Wang, J. Zhou, P. Shen, X. Luo, X. Zhang, J. Ruan, Oncogenic HJURP enhancer promotes the aggressive behavior of triple-negative breast cancer in association with p53/E2F1/FOXM1-axis, Cancer Lett. 611 (2024) 217423.

[75] Z.Q. Qin, Q.G. Li, H. Yi, S.S. Lu, W. Huang, Z.X. Rong, Y.Y. Tang, Z.Q. Xiao, Heterozygous p53-R280T mutation enhances the oncogenicity of NPC cells through activating PI3K-Akt signaling pathway, Front. Oncol. 10 (2020) 104.

[76] A.T.C.C. Yu-Pei Chen, Quynh-Thu Le, Pierre Blanchard, Ying Sun*, Jun Ma, Nasopharyngeal carcinoma, Lancet 394 (2019) 64–80.

[77] Y. Wei, P. Yang, S. Cao, L. Zhao, The combination of curcumin and 5-fluorouracil in cancer therapy, Arch Pharm. Res. (Seoul) (2018) 1–13.

[78] X. Gao, X. Zheng, Y. Zhang, L. Dong, L. Sun, N. Zhao, C. Ding, Z. Ma, Y. Wang, Deficient or R273H and R248W mutations of p53 promote chemoresistance to 5-FU via TCF21/CD44 axis-mediated enhanced stemness in colorectal carcinoma, Front. Cell Dev. Biol. 9 (2021) 788331.

[79] J. Han, J. Li, K. Tang, H. Zhang, B. Guo, N. Hou, C. Huang, miR-338-3p confers 5-fluorouracil resistance in p53 mutant colon cancer cells by targeting the mammalian target of rapamycin, Exp. Cell Res. 360 (2017) 328–336.

[80] F.P. Madorsky Rowdo, G. Xiao, G.F. Khramtsova, J. Nguyen, R. Martini, B. Stonaker, R. Boateng, J.K. Oppong, E.K. Adjei, B. Awuah, I. Kyei, F.S. Aitpillah, M.O. Adinku, K. Ankomah, E.B. Osei-Bonsu, K.K. Gyan, N.K. Altorki, E. Cheng, P. S. Ginter, S. Hoda, L. Newman, O. Elemento, O.I. Olopade, M.B. Davis, M.L. Martin, J. Bargonetti, Patient-derived tumor organoids with p53 mutations, and not wild-type p53, are sensitive to synergistic combination PARP inhibitor treatment, Cancer Lett. 584 (2024) 216608.

[81] C.L. Kuo, S.Y. Wu, S.W. Ip, P.P. Wu, C.S. Yu, J.S. Yang, P.Y. Chen, S.H. Wu, J. G. Chung, Apoptotic death in curcumin-treated NPC-TW 076 human nasopharyngeal carcinoma cells is mediated through the ROS, mitochondrial depolarization and caspase-3-dependent signaling responses, Int. J. Oncol. 39 (2011) 319–328.

[82] H. Ogiwara, A. Ui, B. Shiotani, L. Zou, A. Yasui, T. Kohno, Curcumin suppresses multiple DNA damage response pathways and has potency as a sensitizer to PARP inhibitor, Carcinogenesis 34 (2013) 2486–2497.

[83] N. Chainani-Wu, Safety and anti-inflammatory activity of curcumin: a component of tumeric (Curcuma longa), J. Alternative Compl. Med. 9 (2003) 161–168.
[84] J.C. Ribeiro, A.R. Barnetson, R.J. Fisher, H. Mameghan, P.J. Russell, Relationship between radiation response and p53 status in human bladder cancer cells, Int. J. Radiat. Biol. 72 (1997) 11–20.
[85] C. Lin, Y. Liang, H. Zhu, J. Zhang, X. Zhong, R280T mutation of p53 gene promotes proliferation of human glioma cells through GSK-3β/PTEN pathway, Neurosci. Lett. 529 (2012) 60–65.
[86] D.F. Lee, J. Su, Y.S. Ang, X. Carvajal-Vergara, S. Mulero-Navarro, C.F. Pereira, J. Gingold, H.L. Wang, R. Zhao, A. Sevilla, H. Darr, A.J. Williamson, B. Chang, X. Niu, F. Aguilo, E.R. Flores, Y.P. Sher, M.C. Hung, A.D. Whetton, B.D. Gelb, K. A. Moore, H.W. Snoeck, A. Ma'ayan, C. Schaniel, I.R. Lemischka, Regulation of embryonic and induced pluripotency by aurora kinase-p53 signaling, Cell Stem Cell 11 (2012) 179–194.
[87] Y. Xue, J. Chen, H.H. Choi, L. Phan, P.C. Chou, R. Zhao, H. Yang, J. Santiago, M. Liu, G.E. Yeung, S.C. Yeung, M.H. Lee, HER2-Akt signaling in regulating COP9 signalsome subunit 6 and p53, Cell Cycle 11 (2012) 4181–4190.
[88] D. Zhu, M.F. Huang, A. Xu, X. Gao, Y.W. Huang, T.T.T. Phan, L. Lu, T.Y. Chi, Y. Dai, L.K. Pang, J.A. Gingold, J. Tu, Z. Huo, D.A. Bazer, R. Shoemaker, J. Wang, C. G. Ambrose, J. Shen, J. Kameoka, Z. Zhao, L.L. Wang, Y. Zhang, R. Zhao, D.F. Lee, Systematic transcriptome profiling of hPSC-derived osteoblasts unveils CORIN's mastery in governing osteogenesis through CEBPD modulation, J. Biol. Chem. 300 (2024) 107494.
[89] J. Tu, Z. Huo, Y. Yu, D. Zhu, A. Xu, M.F. Huang, R. Hu, R. Wang, J.A. Gingold, Y. H. Chen, K.L. Tsai, N.R. Forcioli-Conti, S.X.L. Huang, T.R. Webb, J. Su, D.A. Bazer, P. Jia, J.T. Yustein, L.L. Wang, M.C. Hung, Z. Zhao, C.D. Huff, J. Shen, R. Zhao, D. F. Lee, Hereditary retinoblastoma iPSC model reveals aberrant spliceosome function driving bone malignancies, Proc. Natl. Acad. Sci. U. S. A. 119 (2022) e2117857119.
[90] M.V. Kuleshov, M.R. Jones, A.D. Rouillard, N.F. Fernandez, Q. Duan, Z. Wang, S. Koplev, S.L. Jenkins, K.M. Jagodnik, A. Lachmann, M.G. McDermott, C. D. Monteiro, G.W. Gundersen, A. Ma'ayan, Enrichr: a comprehensive gene set enrichment analysis web server 2016 update, Nucleic Acids Res. 44 (2016) W90–W97.
[91] Y. Zhou, B. Zhou, L. Pache, M. Chang, A.H. Khodabakhshi, O. Tanaseichuk, C. Benner, S.K. Chanda, Metascape provides a biologist-oriented resource for the analysis of systems-level datasets, Nat. Commun. 10 (2019) 1523.
[92] A. Xu, M.F. Huang, D. Zhu, J.A. Gingold, D.A. Bazer, B. Chang, D. Wang, C.C. Lai, I. R. Lemischka, R. Zhao, D.F. Lee, LncRNA H19 suppresses Osteosarcomagenesis by regulating snoRNAs and DNA repair protein complexes, Front. Genet. 11 (2020) 611823.
[93] C. Qu, Z. Liang, J. Huang, R. Zhao, C. Su, S. Wang, X. Wang, R. Zhang, M.H. Lee, H. Yang, MiR-205 determines the radioresistance of human nasopharyngeal carcinoma by directly targeting PTEN, Cell Cycle 11 (2012) 785–796.
[94] B.E. Jewell, A. Xu, D. Zhu, M.F. Huang, L. Lu, M. Liu, E.L. Underwood, J.H. Park, H. Fan, J.A. Gingold, R. Zhou, J. Tu, Z. Huo, Y. Liu, W. Jin, Y.H. Chen, Y. Xu, S. H. Chen, N. Rainusso, N.K. Berg, D.A. Bazer, C. Vellano, P. Jones, H.K. Eltzschig, Z. Zhao, B.A. Kaipparettu, R. Zhao, L.L. Wang, D.F. Lee, Patient-derived iPSCs link elevated mitochondrial respiratory complex I function to osteosarcoma in Rothmund-Thomson syndrome, PLoS Genet. 17 (2021) e1009971.